# CINNABAR FOR ROMAN EPHESUS: MATERIAL QUALITY, PROCESSING AND PROVENANCE

Alexandra RODLER-RØRBO, [1,2,3,4]* Anthony J. BARAGONA, [5] Eliah J. VERBEEMEN, [1] Lasse Vilien SØRENSEN, [6] Berk ÇAKMAKOĞLU, [7] Cahit HELVACI, [7] Eduardo BOLEA-FERNANDEZ, [8,9] Ana RUA-IBARZ, [8,9] Frank VANHAECKE, [8] Hilary BECKER, [10] Gilberto ARTIOLI, [11] Lilli ZABRANA, [3] Vinciane DEBAILLE, [2] Nadine MATTIELLI, [2] Steven GODERIS, [1] Philippe CLAEYS [1]

[1] Archaeology, Environmental Changes and Geo-Chemistry, Vrije Universiteit Brussel, VUB, Pleinlaan 2, 1050 Brussels, Belgium

[2] Laboratoire G-time, Department of Geosciences, Environment and Society, Université Libre de Bruxelles, ULB, Avenue F.D. Roosevelt 50, 1050 Brussels, Belgium

[3] Austrian Archaeological Institute of the Austrian Academy of Sciences, Dominikanerbastei 16, 1010 Vienna, Austria

[4] Human Evolution and Archaeological Sciences (HEAS), University of Vienna, Austria

[5] Freelance, Associated with the University of Applied Arts, Vienna, Salzgries 14, 1090 Vienna, Austria

[6] National Museum of Denmark, Frederiksholms Kanal 12, 1220 Copenhagen, Denmark

[7] Department of Geology Engineering, Dokuz Eylül University, Tınaztepe Yerleşkesi, İzmir, Turkey

[8] Atomic and Mass Spectrometry – A&MS research unit, Department of Chemistry, Ghent University, Campus Sterre, Krijgslaan 281-S12, 9000 Ghent, Belgium

[9] Aragón Institute of Engineering Research (I3A), Department of Analytical Chemistry, University of Zaragoza, Zaragoza, Spain

[10] Department of Middle Eastern and Ancient Mediterranean Studies, Binghamton University. State University of New York Binghamton, USA

[11] Department of Geosciences, University of Padua, Via Gradenigo 6, I-35131 Padua, Italy

* Corresponding author: alexandra.rodler-rorbo@oeaw.ac.at; Current address: Austrian Archaeological Institute of the Austrian Academy of Sciences, Dominikanerbastei 16, 1010 Vienna, Austria

## ABSTRACT

Ephesus was an important harbor city that flourished during the Roman period and ancient texts mention Almadén in Spain and the Cilbian fields of Ephesus as important cinnabar sources in antiquity. This work investigates whether imported cinnabar was used and whether this could be related to changes in painting activities over time. Microscopic analysis indicates a consistent preparation of cinnabar, hinting at a uniform source material quality or processing technique. However, the use of cinnabar varies among the architectural structures studied, indicating a plurality of painting techniques. A few of the analyzed cinnabar samples overlap with Turkish- and Balkan reference Pb isotope ratios; three samples from tabernas, however, deviate from this. The Hg isotope ratios reveal that cinnabar from carbonate-hosted deposits was likely used, and that processing of cinnabar included heating as suggested by ancient texts. Most notably, a correlation exists between the geochemical data and the painting technique – shifts in sourcing and cinnabar usage are potentially assignable to building chronology and/or usage. Through the lens of material provenance and processing, Ephesian cinnabar brings the organization of pigment trade into focus.

**Keywords:** Microscopic analysis, Pb isotope ratios**,** Hg isotope ratios, wall paintings, pigment trade

## 1. INTRODUCTION

Various types of mineral pigments were used in Roman art – some of these materials might have been readily accessible, while others were most likely traded. Among the rarest and most highly valued materials used as pigment in antiquity was cinnabar (α-HgS), which was known as *μίνιον* in Greek and *minium* in Latin (inter al. Theophrastus *De Lap.* 58; Vitruvius *De Arch.* 7.8.1-7.9.6; Pliny *HN* 33.37-40; Dioscorides *MM* 5.94 in Beck 2005, 374; Becker, 2022). These terms should not be confused with Indian cinnabar (or dragon's blood (*Indica cinnabaris*) and *minium secundarium* (or red lead, which was also known as *cerussa usta*). Despite the widespread use of pigments throughout history (e.g., Hunt-Ortiz et al., 2011; Cooke et al., 2013; Emslie et al., 2015) and the particularly high demand for various colorants during the Roman period, as evidenced by the rich wall paintings found in both private and public buildings (e.g., Esposito, 2017; Slavdori and Sbrolli, 2021), there is limited knowledge about the organization of pigment production/processing and trade. This is puzzling, considering that ancient authors such as Theophrastus (c. 371–287 BCE) in *De Lapidibus* (*De Lap.*), Vitruvius (c. 80/70–15 BCE) in *De Architectura* (*De arch.*), Pliny the Elder (23/24–79 CE) in *Historia Naturalis (HN)*, and Dioscorides (c. 40–90 CE) in *De Materia Medica* (*MM*), highlight the significance of provenance for the value of ancient pigments. The Cilbian fields of Ephesus and the Almadén mines in Spain were mentioned as the most important cinnabar sources during the Roman period (Gliozzo, 2021); whether Monte Amiata in Grosseto (Italy) or Idrija in Slovenia have been exploited during the Roman period is not certain (Spangenberg et al., 2010). Furthermore, several surveys have already investigated the geology and geochemistry of larger relevant ore bodies in Turkey (e.g., Yıldız and Bailey, 1978; Gemici, 2008; Sayre et al., 2001) and mention for example the Tmolus Mt. near Sardis (Foss and Hanfmann, 1975) or cinnabar outcrops near Selçuk (Schmiesser, 1906). Cinnabar can

occur as a vein mineral, in strata-bound deposits such as in Almadén, Spain, or as secondary mineral in gossans such as in Las Cruces, Spain (e.g., Higueras et al., 2005; Palero-Fernández et al., 2015; Yesares et al., 2017). While ancient texts provide highly valuable clues for evaluating cinnabar provenance, archaeometric analysis – drawing on geological, mineralogical-petrographic and geochemical data – can provide crucial information on material provenance; together these approaches have the potential of providing a way forward for understanding the organization of pigment trade and production networks. The city of Ephesus (present-day Selçuk, south of İzmir, Turkey) developed near the mouth of the Küçük Menderes River on the west coast of Anatolia (for a geochemical discussion of the Ephesian harbor, see Delile et al., 2015). During the Hellenistic and Roman periods, Ephesus emerged as an important trading hub of Asia Minor and the Aegean area. In 188 BCE, Ephesus became part of the Pergamene Empire, leading to significant investments in the reorganization of the harbor and urbanization of Ephesus, which were the foundations for its emergence as an exceptionally important and influential commercial center of the ancient Mediterranean world and its success during the Roman period (Ladstätter, 2016). In 133 BCE, Ephesus became part of the Roman Republic and the capital of the province Asia Minor. Already during the 2$^{nd}$ c. BCE, local artisans began to produce ceramics such as table ware and lamps for exportation (Ladstätter, 2016; Fragnoli et al., 2022). However, despite the significance of Ephesus in the production of ceramic lamps during the Hellenistic period, pottery workshops from this period have not been found so far (Fragnoli et al., 2022). Ephesus was a thriving trade center and a pigment consumer, which raises the question whether this site only imported pigments, or whether processing also occurred here. Currently there is no evidence of pigment production or processing workshops in or near Ephesus, however, this does not necessarily mean that no (local) raw materials were processed for use as painting material. Only a few pigment workshops are currently known for the Hellenistic and Roman periods and their trade networks are still not fully understood. These include sites in the Bay of Naples, Italy (1$^{st}$ c. BCE; e.g., Lazzarini and Verità, 2015), in Memphis, Egypt (1$^{st}$ c. BCE; e.g., Nicholson, 2003), and the late Hellenistic multi-crafting workshop of Kos, Greece (Kostomitsopoulou Marketou, 2019).

Identifying the material quality, processing and provenance of cinnabar can therefore enhance our understanding of ancient pigment workshop practices and the reconstruction of trade routes (e.g., Hunt-Ortiz et al., 2011; Prieto et al., 2015; Rodríguez et al., 2020; Minami et al., 2021). For example, recently, the provenance of cinnabar used in wall paintings in the Roman city of Averticum (Avenches, Vaud, Switzerland) has been investigated suggesting that cinnabar was possibly from the Almadén mining district in Spain (Spangenberg et al., 2010). The analysis of pigment raw materials applies mineralogical/petrographic and geochemical approaches to evaluate possible raw material sources (e.g., Spangenberg et al., 2010; Hunt-Ortiz et al., 2011; Rodler et al., 2017). Geochemical approaches have included lead (Pb) and/or sulphur (S) isotopic analysis as well as mercury (Hg) isotopic analysis (recently reviewed by Gliozzo, 2021). The latter has been used for evaluating which cinnabar deposits were exploited during Andean prehistory (Cooke et al., 2013). Pb is a trace element in sulphur-bearing minerals such as cinnabar, and Pb isotopic analysis has long been used for the provenance study of various inorganic artifacts (e.g., Stos-Gale and Gale, 2009; Artioli et al., 2016). Lead isotopic analysis makes use of the four isotopes of lead $^{204}$Pb, $^{206}$Pb, $^{207}$Pb and $^{208}$Pb that have a natural relative abundance of ca. 1.4 %, 24.1 %, 22.1 % and 52.4 %, respectively (Faure and Mensing, 2005). Of these, only $^{204}$Pb is not radiogenic and its absolute abundance has been stable since the formation of the Earth, while the other three ($^{206}$Pb, $^{207}$Pb and $^{208}$Pb) are formed as end products of radioactive decay from three nuclides, $^{238}$U, $^{235}$U and $^{232}$Th, respectively. The three ratios of each radiogenic isotope to $^{204}$Pb significantly aid in determining the geochronological age of

ore minerals from different deposits. Mercury (Hg) has seven stable isotopes (196−204 amu), which can be affected by both mass-dependent fractionation (MDF, expressed as $\delta^{202}$Hg) and mass-independent fractionation (MIF; expressed as $\Delta^{199}$Hg and $\Delta^{201}$Hg). The MDF of Hg is known to occur during reduction−oxidation reactions, biological cycling, and volatilization of Hg (Blum and Bergquist, 2007). When Hg isotopes undergo MIF, even- and odd-mass-numbered isotopes fractionate from each other; this is most pronounced during UV-induced photochemical reactions (Bergquist and Blum, 2007). Recent research explored the sources of pre-Inca and colonial archaeological cinnabar, as well as the Hg pollution preserved in lake sediment cores in Peru and the Galápagos Islands (Cooke et al., 2013). This research suggested that cinnabar ores from the largest cinnabar-bearing district in Central and Southern America (Huancavelica, Peru) were used. In contrast, cinnabar for Inca artifacts originated from a distinctly different source. Such evaluations can complement the provenance analysis of ores used to manufacture archaeological artifacts.

The aim of this study was to analyze the origin and use of cinnabar in Roman wall paintings found in both private and public houses at Ephesus of the mid-1$^{st}$ to the early 3$^{rd}$ century CE through mineralogical-petrographic and geochemical analyses. This aimed to shed light on changes in material supply and processing, and with this, painting activities organization across different architectural units (likely in a diachronic approach). The evaluation of the origin of the cinnabar used will be aided by making comparisons to available reference data and newly acquired information on cinnabar deposits from the west coast of Turkey, specifically from the Karaburun Peninsula. Overall, this work contributes to the discussion of the organization of pigment trade and processing practices in antiquity.

## 2. MATERIALS AND METHODS

### 2.1. Geological materials

The Karaburun cinnabar mining district consists of three closely associated deposits: Kalecik, Dikencik and Karareis (Fig. 1). These deposits are in the northern part of the Karaburun Peninsula, which is west of İzmir and north of Ephesus. This study includes six samples from these deposits: four from Kalecik and two from Dikencik (examples can be seen in Fig. 2).

Mercury deposits occur in a large variety of rock types, often associated with structural discontinuities. This is also the case for the Karaburun deposits, which can be observed in various geological formations. The oldest rock units in the northern part of the Karaburun Peninsula are represented by relatively autochthonous successions (~495–292 Ma) that consist of clastic sedimentary rocks (Küçükbahçe and Dikendağı Formations) at the western side and various tectonostratigraphic allochthonous units (~245–65 Ma) consisting mainly of carbonates (Gerence, Camiboğazı, Güvercinlik Formations) and flysch deposits (İzmir flysch and Yeniliman serpentinite) at the eastern side (Çakmakoğlu and Bilgin, 2006). These units are unconformably covered by younger rock units of Neogene and Quaternary age (~24 Ma–present) and include volcanic and sedimentary successions (Helvacı et al., 2009; Çakmakoğlu et al., 2013). The ore deposits are epithermal and primarily contain mercury sulphide and quartz crystallized by rising

hydrothermal solutions. The main ore mineral is cinnabar, which occurs as veinlets and fracture fillings in silicified wall rocks (Yıldız and Bailey, 1978). The origin of the cinnabar occurrences is likely related to Neogene volcanism (Yıldız et al., 1967; Helvacı et al., 2009), which introduced mercury-rich solutions into the structural discontinuities of the various formations in the Karaburun Peninsula.

The Kalecik deposit is situated along a channelway through which the rising solutions flowed, following the major northwest-trending fault cutting through the İzmir flysch rocks. The İzmir flysch rocks consist of a sandstone-mudstone dominated matrix and radiolarites, basic volcanic rocks, ultrabasic rocks, and limestone blocks. The ore was likely deposited just beneath the basalt flow unit (Yıldız and Bailey, 1978; Helvacı et al., 2009). In the Dikencik deposit, cinnabar is observed in quartz veins along a fault that silicified the Dikendağı Formation, which includes sand-, silt- and mudstones with black cherts (lydite). The ore zone is approximately 0.7 m wide and 75 m long and is unique in Turkey as it contains a considerable amount of native mercury (Yıldız and Bailey, 1978). The Karareis deposit is very close to the Dikencik mine and is present in the clastic sediments of the Dikendağı Formation. Due to the close proximity to the Dikencik mine and due to cost considerations, no samples from the Karareis deposit were included in this study. The geological materials were collected during fieldwork in 2013 (Fig. 1 and 2). Subsamples of these ore samples were processed for isotopic analysis at Vrije Universiteit Brussel, Université Libre de Bruxelles, and Ghent University, Belgium.

### 2.2. Archaeological materials

The samples drawn from upper painted layers of plasters (as well as cross-sections) were collected from wall painting fragments stored in various boxes at the Ephesus Excavation House of the Austrian Archaeological Institute of the Austrian Academy of Sciences, in Turkey. According to excavation notes, these fragments belong to the southern portal of the Tetragonos Agora (referred to as Agora), as well as to Terrace House 1 and Terrace House 2 (Fig. 3). Some excavation notes also attribute the fragments to specific living units and rooms. However, precise contextualization and dating are challenging. This work uses the excavation notes, descriptions of living units/rooms, and available information about building periods, to provide all the available information about the samples. The samples were collected from wall painting fragments from Terrace House 1 (Taberna IV), various living units and rooms of Terrace House 2 (including a taberna adjacent to Living Unit 7), and wall painting fragments from the Agora. However, the samples were not collected from walls still *in situ* in various Roman houses introducing an uncertainty regarding building structure and periods. These samples more generally represent cinnabar pigments from Roman Ephesus.

The top layer of wall painting fragments (e.g., Fig. 2) was first analyzed using the handheld energy-dispersive X-ray fluorescence (HH-EDXRF) spectrometer Olympus InnovX Delta Premium 6000 (Rh anode, 8-40 keV, Si-drift detector, 4W X-ray tube, current range of 5-200 μA). Based on this semi-quantitative *in situ* analysis of major and trace elements, wall painting fragments were selected on-site for sample collection and further analysis.

The insula houses Terrace House 1 and Terrace House 2 were excavated amidst the remains of Ephesus. Terrace House 1 covers an area of ~3,000 $m^2$ and consists of several living units, each containing multiple

rooms. Terrace House 2 covers an area of ~4,000 $m^2$; it consists of seven living units. Both insula houses were built in the first century CE and subsequently destroyed during an earthquake in 262/263 CE (Thür and Rathmayr, 2014; Delile et al., 2015). The samples from Terrace House 1 pertain to Taberna IV. Renovation works were undertaken in Terrace House 1 following an earthquake ($2^{nd}$ period, ~17–140 CE; Lang-Auinger and Outschar, 1996). The samples are likely pertaining to this renovation period. The samples from the Tetragonos Agora are from the Southern portal. The samples from Terrace House 2 pertain to the Taberna adjacent to Living Unit 7 (Room 45), as well as to Room 36 of Living Unit 6, Room 12 of Living Unit 3, and Room 21 of Living Unit 4. Wall paintings with cinnabar were discovered in Room 36 and 31b, leading to the proposal that these would represent an early painting phase (Thür and Rathmayr, 2014). The building phases in Terrace House 2 are categorized into four groups spanning from the mid-$1^{st}$ c. CE to the early $3^{rd}$ c. CE (Zimmermann, 2005).

Stratigraphic wall painting cross-sections, and scrapings of the top pigment layer, were collected with a saw and scalpel, respectively. Of the wall painting fragments collected, ten (four from Terrace House 2, two from Terrace House 1, and four from the Agora) were processed into polished petrographic cross-sections to study plaster and paint layer stratigraphy. All samples were obtained from large sections of monochrome red wall paintings, although occasionally other hues were visible (e.g., EPHCIN-20 and -26; Fig. 2). The pigment powders were processed at Vrije Universiteit Brussel, Université Libre de Bruxelles, and Ghent University for isotopic analysis.

### 2.3. Cross-sections: optical microscopy and SEM-BSE/EDX

To study the morphology of cinnabar pigment and its application on painted surfaces, the plaster fragments processed as cross-sections were examined using both light microscopy and SEM-BSE/EDX. This examination was conducted on unprocessed fragments as well as on those prepared as stratigraphic polished cross-sections. For incident light microscopy, a Nikon SMZ 1500 stereomicroscope was used. In addition to optical microscopy, SEM analysis was performed under high vacuum conditions, using an accelerating voltage of 15-25 kV in back-scattered electron (BSE) detection mode on the cross-sections to provide a clearer view of cinnabar morphology and its distribution within the samples. Cinnabar appears brighter in SEM-BSE images relative to red and/or yellow ochre owing to the higher atomic mass; this was exploited to create images in which only the cinnabar grains are visible by radically adjusting the brightness/exposure until the ochre grains no longer are visible. This can be verified since there are corresponding light microscopy images showing the location of both cinnabar and ochre pigment grains concentrated in separate paint layers in the same samples; once the known ochre layers disappear from the image, it is assumed that only cinnabar remains in the BSE image. This allows the exclusive study of cinnabar, including quantitative grain size and distribution image analysis with Image-J freeware (which was also performed on SEM-BSE images of the surface of painting fragments before processing into cross sections). Semi-quantitative EDX analysis of 20 grains of cinnabar per sample, thus isolated, was performed in support of the more precise and specific chemical analyses described below. The SEM-BSE/EDX analysis was performed at the University of Applied Arts Vienna using a Quanta FEG 250 (FEI, U.S.A.) scanning electron microscope coupled to the Octane Elect Plus EDX detector (Ametek/EDAX, U.S.A.) and equipped with Genesis EDX Quant software.

## 2.4. Isotopic analysis

Subsamples (a few mg) of the collected top pigment layers (consisting of cinnabar and red clays, see 3.1) and the geological samples from the Karaburun deposits were fully digested in *aqua regia* under a 100-class flow hood at the G-Time laboratories at Université Libre de Bruxelles. Lead was chromatographically isolated from the digested geological and archaeological samples using the anion exchange Biorad™ AG1-X8 resin (mesh size of 100-200 µm). Lead was separated from the matrix elements using a standard protocol based on the use of HBr-HCl (Vanderstraeten et al., 2020). After the purified Pb eluent fractions were obtained and evaporated to dryness, they were dissolved in 100 µl of concentrated $HNO_3$, evaporated and finally dissolved in 0.05% $HNO_3$, for subsequent isotopic analysis using a Nu Plasma II (Nu II) high-resolution multi-collector inductively-coupled-plasma mass-spectrometry (HR-MC-ICP-MS) instrument from Nu Instruments at the Laboratoire G-time, Université Libre de Bruxelles.

A thallium standard solution (Alpha ICP standard) used as a dopant - with a known $^{205}Tl/^{203}Tl$ isotope ratio of 2.3871 - was added to all sample and standard solutions. Solutions were prepared to obtain a Pb-Tl ratio of 4 or 5, and a minimum signal of 100 mV in the axial collector for $^{204}Pb$ (*i.e.*, the concentrations were controlled to get 200 ppb of Pb and 50 ppb of Tl). A combination of internal correction based on the monitoring of the Tl isotope ratio and external correction with the standard measured in a sample-standard bracketing (SSB) approach was applied to correct for the bias induced by instrumental mass discrimination for the measured Pb isotope ratios. Isobaric interference on mass 204 due to potentially present $^{204}Hg$ was monitored during acquisition by measuring the signal intensity at an m/z = 202 (Weis et al., 2006; Vanderstraeten et al., 2020). While the Pb total beam was at ~8 V, the $^{202}Hg$ beam intensity remained below 3 mV. The corrected Pb isotope ratios are reported using the recommended values of Abouchami et al. (2000) for the Pb isotopic reference material NIST SRM 981.

A solution of the isotopic reference material NIST SRM 981 Pb standard solution was routinely analyzed before starting a sample batch, as well as between every two samples to assess precision and reproducibility; repeated analyses of NIST SRM 981 provided mean values of 16.941 ± 0.004, 15.501 ± 0.005 and 36.716 ± 0.015 (2SD, n=26) for $^{206}Pb/^{204}Pb$, $^{207}Pb/^{204}Pb$ and $^{208}Pb/^{204}Pb$, respectively. These results are in line with the long-term repeatability of NIST SRM 981 values at the Laboratoire G-time of 16.9407 ± 0.0036, 15.4968 ± 0.0047 and 36.7163 ± 0.0121 (2SD, n=167; Vanderstraeten et al., 2020) for $^{206}Pb/^{204}Pb$, $^{207}Pb/^{204}Pb$ and $^{208}Pb/^{204}Pb$, respectively, and with the data reported by (Weis et al., 2005). Six samples were analyzed in duplicate (EPHCIN-17, -19, -20, -27; EPHCINO-04 and -05), and the data repeatability was within two standard deviations (2SD) for all samples. The procedural blank contained a Pb amount of 5 ng (n=1), which is significantly lower (<5%) than the sample Pb contents and thus not expected to affect the Pb isotope ratio results. The blank contribution to individual samples was <0.1%.

The isotopic analysis of Hg was carried out using a Neptune MC-ICP-MS unit from Thermo Fisher Scientific at Ghent University. Hg was introduced as Hg(0) generated *via* the selective reduction of $Hg^{2+}$ with 3% $SnCl_2.2H_2O$ in 1.2 M HCl in an HGX-200 cold vapor and hydride generation unit (Teledyne Cetac Technologies, USA). The Hg(0)-loaded carrier gas coming from the cold-vapor generation (CVG) unit was admixed in a 'T' piece with a wet aerosol of Tl generated by using a 100 µL $min^{-1}$ concentric nebulizer

mounted onto a dual (cyclonic and Scott-type) spray chamber (this setup is described in detail elsewhere: Rua-Ibarz et al., 2016a,b, 2019; Bolea-Fernandez et al., 2019).

For instrumental mass discrimination correction, like for Pb isotopic analysis, a combination of internal correction using Tl as admixed internal standard (NIST SRM 997 - Tl) in a "Baxter approach" and external correction (NIST SRM 3133 - Hg) with the SSB-approach was used (Baxter et al., 2006). An in-house standard solution of Hg previously characterized for its isotopic composition was measured in-between the samples for Quality Assurance and Quality Control (QA/QC). Using NIST SRM 3233 (Hg), the external precision was calculated to be ≤0.12 ‰ (2SD; over a period of 18 months, n=250; Rua-Ibarz et al., 2016a). This precision is sufficient for studying the natural isotope ratio variation of Hg. To obtain accurate results, the Hg concentration and acid content of all samples and standards were matched within ± 10 %. Blank subtraction was not applied because the effect of the blank was demonstrated to be negligible within the experimental precision.

Hg isotope ratios are reported as delta ($\delta^{xxx}$Hg) values. To separate the effect of MIF on the Hg isotope ratio from that of MDF, the contribution caused by MDF is subtracted from the experimentally determined $\delta^{xxx}$Hg values using the equations below. Both delta and capital delta values are reported in per mil (‰) (Blum and Bergquist, 2007).

$$\partial^{xxx}Hg\ (‰) = \left(\frac{\left(^{xxx}Hg/^{198}Hg\right)_{sample}}{\left(^{xxx}Hg/^{198}Hg\right)_{NIST\ SRM\ 3133}} - 1\right) * 1000$$

where xxx = 199, 200, 201 or 202 and NIST SRM 3133 is the Hg isotopic reference material.

$$\Delta^{199}Hg = \partial^{199}Hg - \left(\partial^{202}Hg * 0.2520\right)$$
$$\Delta^{201}Hg = \partial^{201}Hg - \left(\partial^{202}Hg * 0.7520\right)$$

## 3. RESULTS

### 3.1. Material processing, pigment layers and painting techniques

Visual examination of the wall painting fragments from Ephesus and optical microscopy (OM) shows a similar appearance. However, a closer examination beneath the surface of the 10 cross-section samples reveals technical details not immediately evident through visual inspection or non-invasive analysis. Figure 4 shows four examples of these cross-sections as examined by OM, along with SEM/EDX micrographs of pigment layers with the exposure adjusted to highlight the cinnabar grains only. These images display four different painting applications / cinnabar usage described below; each of the 10 cross sections fit into this typology. They are:

*Technique 1* (Agora) (samples EPHCIN-26, -28): Figure 4A shows a sample taken from the Tetragonos Agora, where a thin (± 25 µm) layer of cinnabar was applied over an ochre layer applied *a secco* - ochre

paint has seeped into drying cracks. The granulometry of this sample also indicates the use of a coarser pigment (average particle size 8.5 μm, site average of 5.8 μm; Tab. 1).

*Technique 2* (TH1) (samples EPHCIN-20, -24): Figure 4B, representing a sample from Terrace House 1, displays a pigment layer over 100 μm thick, consisting of 2 layers of ochre, one yellow and one red, topped by a thin layer of cinnabar.

*Technique 3* (TH2A) (samples EPHCIN-05, -06, -14, -18): Figure 4C shows a sample from Terrace House 2, exhibits a clearly distinct technique from that of Terrace House 1; it shows a two-layer system of cinnabar mixed with ochre over an ochre underpainting around 100 μm thick.

*Technique 4* (TH2B (samples EPHCIN-21, -25): Figure 4D shows a second technique from Terrace House 2; it displays a thick (±75 μm) layer containing cinnabar pigment only, over an ochre-tinted intonaco layer. Additionally, the sample in Figure 4D contains an ochre-tinted intonaco layer roughly 5 mm below the finished surface.

Despite the difference in ochre underpainting between *Techniques 2* and *4*, there are also some similarities. The visual resemblance is apparent in both techniques (Fig. 4B, D), which use a significant amount of cinnabar, but digital image analysis reveals that the grain size distribution of the cinnabar is quite similar. In contrast, *Technique 3* (Fig. 4C) shows that not only was less cinnabar used, which is visually apparent as well as supported by an average particle spatial distribution of 7 μm, but it also tended to be a finer grade of pigment (Tab. 1).

### 3.2. Element and isotope ratio data

EDX analysis on a representative number of cinnabar grains in all 10 cross-sectioned samples, provided semi-quantitative elemental characterization. The stoichiometry of the cinnabar used at the site appears relatively similar, with any differences in the mercury-to-sulphur balance attributed to other elemental "impurities" affecting this balance. Trace amounts of As and Se are present in the cinnabar grains of the samples analyzed, at slightly different levels from sample to sample. Broadly speaking, in samples of painting *Technique 3* the signal for As and Se was at or below the margin of error for the detection limit, i.e., they could not be determined to be present. Samples from *Technique 4* had the highest levels of these elements detected, equivalent to about a ratio of 200:1 S:As, 400:1 S:Se – too low for definite quantification, but far enough above the background signal to be determined to be present. The cinnabar grains of the other two techniques (*1 and 2*) had average levels of As and Se roughly half that of *Technique 4*. An important caveat to this is that some grains had no As or Se detectable, while others had levels as high as *Technique 4*, which may indicate pigment mixing. However, due to the low levels detected and limitations of the method, it is generally advisable to defer to the results of geochemical testing described that follows. Despite the possibility for contamination in these samples and others, it is expected that the Pb and Hg contents (and their respective isotope ratios) accurately reflect the visually identified cinnabar.

The Pb isotope ratios of the Karaburun ores (n=8) fall within the range 18.96 - 19.46 (± 0.01, 2SD) for $^{206}Pb/^{204}Pb$, 15.70 - 15.72 (± 0.01, 2SD) for $^{207}Pb/^{204}Pb$, and 38.62 - 38.99 (± 0.02, 2SD) for $^{208}Pb/^{204}Pb$ (Tab. 2). The Pb isotope ratios of the Ephesian pigment samples (n=18) vary between 18.24 and 18.82 (± 0.01, 2SD) for $^{206}Pb/^{204}Pb$, 15.63 and 15.69 (± 0.01, 2SD) for $^{207}Pb/^{204}Pb$, and between 38.27 and 38.96 (±

0.02, 2SD) for $^{208}Pb/^{204}Pb$ (Tab. 2). Among the fourteen cinnabar samples analyzed, eleven exhibit similar Pb isotope ratios, while the remaining three samples show distinctly lower values across all three Pb isotope ratios. These three pigment samples originate from wall painting fragments found in Terrace House 1 (EPHCIN-23, -24) and Room 45 of Terrace House 2 (EPHCIN-25); the $^{207}Pb/^{206}Pb$ and $^{208}Pb/^{206}Pb$ ratios of these samples are between 0.8451 ± 0.0001 and 0.8569 ± 0.0003 (± 2SD), and between 2.0813 ± 0.0004 and 2.0973 ± 0.0006 (± 2SD), respectively (Tab. 2). These results of cinnabar pigment samples from Ephesus were first compared to previously reported cinnabar pigment and ore samples by Mazzocchin et al. (2008), Hunt-Ortiz et al. (2011), and Rodríguez et al. (2020), and plotted with the available Pb isotope ratio data (Fig. 5). This was followed by a statistical compilation of the dataset based on calculation of the Euclidean distances between pigment and cinnabar ore samples compared to reference Pb isotope ratio data using the AAcP Pb isotope ratio database (Artioli et al., 2016) for evaluating potential cinnabar source areas (Fig. 6). This was focused on comparing to ore deposits with known cinnabar mineralization. Pb isotope ratio data of cinnabar pigment samples should be first and foremost compared to Pb isotope ratio data of cinnabar ore deposits as this is more appropriate than comparing to lead-bearing minerals (Higueras et al., 2005; Minami et al., 2021). However, reference Pb isotope ratio data for potentially relevant cinnabar ore deposits, such as those of Chios (Greece) or at the Black Sea Coast (e.g., Georgia) are currently not available for comparison.

The mercury isotopic composition (i.e., $\delta^{199}Hg$, $\delta^{202}Hg$, $\Delta^{199}Hg$ and $\Delta^{201}Hg$) of six pigment and three ore samples was characterized. The mercury isotope ratio data for Kalecik ore samples are characterized by $\delta^{202}Hg$ values of -0.23 and +0.12 ‰ and $\Delta^{199}Hg$ values of -0.15 and -0.22 ‰ (n=2; Tab. 2), while the ore sample from Dikencik is characterized by a $\delta^{202}Hg$ value of -0.05 ‰ and a $\Delta^{199}Hg$ value of -0.05 ‰ (n=1; Tab. 2). Among the pigment samples, three (EPHCIN-13, -24, -27; Tab. 2) cluster closely with $\delta^{202}Hg$ values ranging from +0.62 to +0.79 ‰ and $\Delta^{199}Hg$ values ranging from -0.09 to -0.13 ‰ (Fig. 7). The remaining three samples (EPHCIN-06, -25, -26) have $\delta^{202}Hg$ values of +1.13 ‰, +1.07 ‰ and +0.66 ‰ and $\Delta^{199}Hg$ values of -0.13 ‰, -0.40 ‰ and -0.31 ‰, respectively, and the analytical precision is ≤0.12 ‰ (2SD; n=250; Rua-Ibarz et al., 2016a).

A brief description and overview of the sample groupings according to material processing, painting techniques and geochemical results along with the archaeological contexts is listed in Table 3.

## 4. DISCUSSION

Trade in pigments was mentioned in ancient texts, yet little is currently known about the organization of pigment trade and production networks in antiquity (Becker, 2021, *forthcoming*). Several ancient authors mentioned pigment use, provenance, and processing, as discussed in a recent review on cinnabar (Gliozzo, 2021). Briefly, Theophrastus wrote that cinnabar was ground in stone- and washed in copper vessels (*De Lap.* 58; c. 315–305 BCE). Similarly, Vitruvius mentioned that cinnabar was prepared by repeatedly being ground and washed to a powder to separate it from mercury (*De Arch.* 7.9.1; 1st c. BCE). According to Pliny (*HN* 33.37; c. 77–79 CE), cinnabar was extracted from red sand found in silver mines. Like Vitruvius, Pliny described repeated grinding and washing to obtain a high-quality cinnabar. However, there are currently no

cinnabar pigment production or processing workshops known from the archaeological record. The investigation of pigment processing and its organization therefore rests on the available evidence such as wall paintings and other use contexts. The initial visual examinations of the wall painting fragments from Roman Ephesus prior to making cross-sections suggested a consistent appearance. SEM images generally show similar pigment grain morphology across different samples, and the stoichiometry of the cinnabar used (*i.e.*, here Hg:S ratio) is consistent among the samples analyzed (Tab. 1). This might be indicative of material from similar sources (Maras et al., 2013; Gliozzo, 2021).

Photomicrographs of cross-sections from the Agora, Terrace House 1 and 2 (Fig. 4), however, revealed different painting techniques that can be attributed to different painting activities and/or time periods. A similar observation was recently made regarding the use of cinnabar in Roman Noricum (mostly present-day Austria and Slovenia), where different painting techniques were used in roughly contemporaneous sites, likely representing different painting activities, different representations the artists wanted to paint and/or resource levels of the patrons (Baragona et al., 2022). The results of this work suggest at least two painting phases: one involving *Technique 1* and *3*, and another involving *Technique 2* and *4* (Tab. 3). There may also be a 3rd phase associated with the deeper ochre-tinted intonaco in *Technique 4*, possibly indicating later replastering and repainting. As for other sites, differences in painting techniques can possibly be attributed to processing by different painting activities, which might have implications for the diversity of workshops and/or artists expressions in these periods.

A sample taken from the Tetragonos Agora (*Technique 1*) displays a thin layer of relatively large-grained cinnabar pigments mixed with ochre. However, whether this appearance is due to weathering or differences in resource allocation by the artists remains uncertain. Furthermore, *Technique 3* of Terrace House 2 is similar to the example from the Agora (*Technique 1*), but it features thicker pigment layers and a finer-grade cinnabar. While these techniques are similar and might have used comparable raw materials, as suggested by the Pb isotopic analysis (see *4.2*; Fig. 6), phase chronology is unclear and the relationship between *Technique 1* and *3* cannot be fully established at this point. However, this might be possible for *Technique 2* and *4*. A similar effect with cinnabar over yellow ochre on top of an ochre-tinted *intonachino* as seen in Taberna IV of Terrace House 1 at Ephesus (*Technique 2*) was also observed in Noricum from a likely mid-2nd century CE structure (Baragona et al., 2022). Furthermore, imagery of the sample from the Taberna adjacent to Terrace House 2 (Room 45, *Technique 4*) displays a thicker cinnabar layer with no red ochre underpainting and shows the final millimeters of intonaco have red ochre added (as opposed to ochre underpainting) and a second ochre-tinted intonaco layer 5 mm below the first, indicating a re-painting campaign. The practice of adding ochre to the final layer of the intonachino has been previously reported at other sites, for example at Ostia Antica, and is associated with wall paintings of the 4th Pompeiian style (mid-1st to early 2nd century CE) (Esposito, 2014; Bracci et al., 2021). Cinnabar granulometry, as determined by EDX analysis, as well as Pb isotopic analysis reveals similarities between *Technique 2* and *4*, that hint at similar material processing by the painting activities and/or a painting period. There is increasing evidence that stylistic changes over time were similar empire-wide (Tober, 2021), which might have influenced the organization of painting workshops. The following sections demonstrate how these differences can also be linked to geochemical data and, consequently, to the organization of the trade networks that supplied cinnabar for Ephesus.

The advantageous location of Ephesus, on the west coast of Asia Minor, made it a significant cultural and communication center during the Roman period (Delile et al., 2015). The site's location enabled access to

natural resources and products, such as control over the trade of certain pigments (e.g., Tezgör, 2022). Theophrastus mentions the use of natural cinnabar found in Iberia and in Colchis at the Black Sea (Gliozzo, 2021): cinnabar from a location 'above' Ephesus was prepared from sand that shone brightly and resembled scarlet dye (*i.e*., kermes) (*De Lap.* 58). In agreement with Theophrastus, Vitruvius also mentioned that cinnabar was first discovered in the Cilbian fields near Ephesus (*De Arch.* 7.8.1). Pliny agreed with both Theophrastus and Vitruvius, stating that a hard and sandy kind of cinnabar came from Spain and the region of the Colchi, while the highest-quality cinnabar used for painting could be found in the Cilbian territory beyond Ephesus (*HN* 33.37; 39). Dioscorides mentioned Libya as the place of origin for high-quality and expensive cinnabar, while emphasizing the Cilbian fields of Ephesus and the Almadén mines in Spain as the most important cinnabar mines (*MM* 5.94; c. 50-70 CE; Beck, 2005). Cilbian is the area north and east of the ancient city of Larisa on the Tmolos and extends to present-day Kiraz in the east (Keil and Premerstein 1914; Meriç 2009; Zabrana 2022). A rock inscription from the 3rd c. CE (Keil and Premerstein 1914) and near today's Emirli might identify this area as belonging to the city of Ephesus and might furthermore connect it with the Cilbian territory (Zabrana 2022).

From previous works, several cinnabar sources are known in Turkey. For example, the preliminary survey of mineral resources by Foss and Hanfmann lists cinnabar ore deposits in Tmolus Mt., located ~20 km from Sardis. Ancient workings above the village of Ayasuluk (possibly the ancient Nicaea of the Cilbiani) in the Cayster Valley were documented there (Foss and Hanfmann, 1975:21). Modern workings were also observed south of the village of Allahdiyen, visible from the mountain road connecting Sardis to Ödemiş. The work by the German geologist Carl Schmeisser had previously mentioned mercury/cinnabar occurrences in Turkey; one crops out in quartz-bearing slate and is located near the village Habibler, ~20 km northeast of Selçuk, and the other in clay-rich sedimentary deposits in the Kaystros Valley near the village Haliköy, ~85 km northeast of Selçuk (Schmiesser, 1906). Additionally, cinnabar deposits within the İzmir province are located near Ulubey, Alaşehir and Ödemiş. The geology (Yıldız and Bailey, 1978; Gemici and Oyman, 2003; Gemici, 2008) and geochemistry (Gale and Stos-Gale, 1981; Wagner et al., 1985; Yener et al., 1991; Hirao et al., 1995; Sayre et al., 2001; Hauptmann et al., 2002; Begemann et all., 2003; Willett and Sayre, 2006; Gökce and Bozkaya, 2007) of ore deposits in Turkey have been extensively investigated before, facilitating a comparison with the new data included in this study while the focus was to compare to ore bodies with cinnabar mineralization included in the AAcP database (see 3.2.).

While the Pb isotope ratio data of the Ephesian cinnabar samples roughly fall into two groups: (i) two samples from Taberna IV of Terrace House 1 and one sample from Room 45, which is part of the Taberna adjacent to Living Unit 7 of Terrace House 2, and (ii) the remaining samples from Terrace House 2 and the Agora. The Pb isotope ratio data of the Karaburun cinnabar ores do not align with those of the Ephesian cinnabar samples, and thus, cannot be considered as the source of cinnabar to Ephesus; other ore deposits appear to be a better fit. Perhaps (a mixture of) cinnabar from different source areas might have been used, as previously proposed for cinnabar samples from Roman wall paintings (Mazzocchin et al., 2008). The work by Mazzocchin et al. (2008) proposed that cinnabar from various sources – such as Huelva (Rio Tinto) and Almeria, Spain, as well as other mining districts in southern Spain that were exploited by the Romans – might have been mixed at a hitherto unknown production or processing workshop in Rome before the pigments were used at various Roman sites. Interestingly, Vitruvius specifically recorded that cinnabar from Spain was processed in a workshop there (*De Arch*. 7.9.4); in such a workshop environment, cinnabar collected from different sources in Spain could have been intermixed. This might be supported by overlaps

of previously published Pb isotope ratio data for cinnabar pigments (Mazzocchin et al., 2008; Hunt-Ortiz et al., 2011; Rodríguez et al., 2020) and Ephesian cinnabar pigments (Fig. 5A).

Furthermore, it was suggested that cinnabar from Almadén, Spain, was used for wall paintings in the Roman city of Aventicum (Avenches, CH) on the basis of sulphur isotopic analysis for comparing relevant European mining districts (Spangenberg et al., 2010). In this work, samples from Almadén were the closest match for the cinnabar used in Aventicum. However, it was also noted that cinnabar from various sources might have been brought to Rome and mixed there before being used (Spangenberg et al., 2010). While some Ephesian samples overlap with cinnabar from Almadén, for most of them there is a good match with reference samples from the Taurus Mts in Turkey or from Balkan sources. However, the possibility of mixtures from various sources remains plausible (Mazzocchin et al., 2008; Spangenberg et al., 2010) – for example, the $^{207}Pb/^{206}Pb$ ratio of Terrace House 1 samples points in this direction: $^{207}Pb/^{206}Pb$ ratios between 0.847 and 0.856 correspond to the gap between the Variscan and the precursors of the Alpine orogeny in Europe, when there were only a few ore-forming events; Pb isotope ratios that plot within this gap therefore likely result from mixing (Klein et al., 2004). Furthermore, potential source areas such as Chios (Greece) or the Black Sea Coast of Georgia could not be considered due to the current lack of reference data. As shown for lead and copper ore deposits (Klein et al., 2009) and noted previously (Spangenberg et al., 2010), cinnabar from different Hg-mineralized bodies within mining districts could be characterized by heterogeneous isotope ratios, potentially contributing to a wider range in sample isotope ratios and necessitating careful data interpretation.

With regards to the Hg isotope ratio data, it seems likely that cinnabar from sedimentary exhalative deposits was used. While cinnabar sources need to be carefully characterized (Stephens et al., 2021), this provides additional insights for assessing material provenance and for enriching reference databases. Briefly, hydrothermal ore deposits exhibit a wide intra-deposit range in $\delta^{202}Hg$ values (Yin et al., 2016). The level of MIF as reflected by the $\Delta^{199}Hg$ values is low (Fig. 7A). The $\Delta^{199}Hg$ values of the samples analyzed ranged between -0.09 ‰ and -0.13 ‰ for the larger Pb isotope ratio cluster of samples mainly from Terrace House 2. These values closely resemble those observed for sedimentary exhalative deposits ($\Delta^{199}Hg$: -0.09 ± 0.18 ‰; Yin et al., 2016). The Karaburun deposits are sedimentary exhalative deposits, but similar to the Pb isotope ratio data, there is no overlap between pigment and Karaburun ore Hg isotope ratios. However, while the use of high-temperature conditions does not induce Hg isotope MIF (Chen et al., 2022), MDF may occur during ore roasting processes (Ni et al., 2022) as indicated by recent laboratory roasting of cinnabar ore from Almadén (Gray et al., 2013). This MDF can be the result of several complex geochemical processes involved during roasting which include redox processes, vapor transport, and secondary mineral formation (Smith et al., 2014) and was observed in a small laboratory experiment during retorting (Gray et al., 2013). The $\delta^{202}Hg$ values obtained for the pigment samples (0.62 ‰ to 1.13 ‰) are higher than those corresponding to the Karaburun ore samples (-0.23 ‰ to 0.12 ‰). If cinnabar from these ores would have been used, then this could be in agreement with the loss of isotopically lighter Hg isotopes under high-temperature conditions. This might apply to cinnabar pigments from Ephesus, where the $\delta^{202}Hg$ values are not within the range reported for cinnabar from Almadén (-0.92 to 0.15 ‰, n=7; Gray et al. 2013; -1.73 to 0.15 ‰, n=18; Pribil et al., 2020). However, the use of Karaburun or Almadén ores (in cinnabar pigment mixtures) cannot be excluded based on the Pb isotopic analysis alone and either might be a possibility based on the Hg isotope ratio data.

Cinnabar was a highly valued colorant and several historical sources mention the ore deposits of Almadén and ore deposits near Ephesus as source areas. Recent research used Pb, S and Hg isotope ratio data of cinnabar from archaeological contexts to evaluate cinnabar provenance and potential trade contacts (Mazzocchin et al., 2008; Spangenberg et al., 2010; Hunt-Ortiz et al., 2011; Tsantini et al., 2018; Rodríguez et al., 2020; Minami et al., 2021). This work contributes cinnabar samples from ancient wall paintings from Ephesus and cinnabar ore from nearby deposits and uses Pb as well as Hg isotope ratio data to evaluate material provenance, trade and processing. However, future research would benefit from a more detailed evaluation of mixing with other pigments (Rodríguez et al., 2020) and building on first laboratory experiments (Gray et al., 2013), further research is necessary to characterize the effect of ancient cinnabar processing on the Hg isotopic composition of cinnabar pigments. This is needed in order to better compare archaeological with geological materials and to substantiate a potential MDF due to heat treatment. If cinnabar processing treatments influence trace element partitioning or isotope fractionation, then this would be relevant for such an interpretation. Furthermore, comparing geochemical results of ancient pigments to a wider range of possible source areas would significantly advance pigment provenance studies. This work contributes new cinnabar ore samples and emphasizes that several potential source areas are currently not available for comparison. The lack of cinnabar processing sites in the archaeological record complicates this further. In general, only a few pigment workshops are currently known (e.g., Kostomitsopoulou Marketou & Rodler-Rørbo, 2023). An archaeometric investigation of such workshops (Kostomitsopoulou Marketou, 2019; Kostomitsopoulou Marketou et al., 2020) is helpful for evaluating pigment preparation methods, for example, in comparison to ancient literary evidence, and can aid an interpretation of possible trade routes. Further investigations of Hg paleopollution in sedimentary deposits might be useful in this regard (Cooke et al., 2013); further analysis of cinnabar pigments to add to the already existing data (Fig. 5A) and minor cinnabar deposits should be considered and included in future studies (Rodríguez et al., 2020) to expand the currently available data (Fig. 5B).

## 5. CONCLUSION

In conclusion, this work aimed to determine whether raw materials from the Karaburun Peninsula north of Ephesus, from the Spanish Almadén mining district, or from other close or distant cinnabar sources were used at Ephesus. Analysis using optical and scanning electron microscopy of the paint layer stratigraphy, as well as cinnabar grain size distribution, indicated consistent cinnabar pigment preparation. While this could suggest uniform source material quality, it could also indicate a relatively consistent (although likely diachronic) material processing technique. However, variations in paint layer stratigraphy among different architectural structures suggest a diversity of painting techniques over time. A correlation between painting technique and geochemical information was observed, implying changes in cinnabar source and pigment preparation, possibly associated with changes in building chronology and/or usage. Although the Pb isotope ratio data of the majority of the Terrace House 2 and the Agora samples cluster closely together and align well with Balkan or central Turkish ore deposits, a small subset of samples – all from tabernas adjacent to either Terrace House 1 (Taberna IV) or Terrace House 2 (Room 45, adjacent to Living Unit 7) – suggests different sources. However, while Turkish ore deposits are well-represented in reference databases, several potentially relevant cinnabar deposits have not yet been included (e.g., Chios, Greece; Black Sea Coast,

Georgia). Additionally, the possibility of cinnabar mixing from various sources remains plausible. The Hg isotope ratio data of Ephesian pigment samples consistently shows the loss of isotopically lighter Hg isotopes. However, additional research is necessary to evaluate whether this could indicate heat treatment during pigment processing as suggested by ancient authors.

## ACKNOWLEDGMENTS

We thank Pamela Fragnoli and Sabine Ladstätter, Austrian Archaeological Institute of the Austrian Academy of Sciences, for supporting this project and the fieldwork in Ephesus, and to all those that excavated this marvelous site in the past. The Turkish authorities kindly granted the research permits that enabled sample collection and analysis; we are grateful for this. We thank Wendy Debouge and Jeroen De Jong, Université Libre de Bruxelles (BE), for keeping the laboratory in perfect shape and for support with mass spectrometry. We also thank Verena Fugger of the Austrian Archaeological Institute of the Austrian Academy of Sciences, for comments about ancient texts and recent geological surveys. Moreover, A.R.R. thanks the Austrian Archaeological Institute of the Austrian Academy of Sciences for a generous travel fund for fieldwork as well as the Holzhausen Legat of the Austrian Academy of Sciences for supporting finalizing this manuscript. Furthermore, A.R.R., S.G., V.D. and F.V. acknowledge support from the FWO-FNRS EoS program "ET-HoME". V.D. also thanks the FRS-FNRS for present support. E.B.-F. acknowledges financial support from the Ramón y Cajal programme (RYC2021-031093-I) funded by MCIN/AEI/10.13039/501100011033 and the European Union (NextGenerationEU/PRTR), the grant PID2021-122455NB-I00, funded by MCIN/AEI/ 10.13039/501100011033 and by "ERDF A way of making Europe", and the Aragon Government (DGA, Construyendo Europa desde Aragón, Grupo E43_20R). A.R-I thanks European Union´s Horizon 2020 research and innovation program under the Marie-Sklodowska-Curie grant agreement Nº 101034288. F.V. acknowledges FWO-Vlaanderen for providing the funding for the acquisition of MC-ICP-MS instrumentation (ZW15-02 – G0H6216N). L.V.S. thanks The Carlsberg Foundation (CF14-0280) for their support in financing his postdoctoral research of rare raw materials in the Aegean. Furthermore, we thank four anonymous reviewers for their comments that improved this work.

**Author contributions:** Conceptualization, A.R.R.; sample collection, A.R.R., L.V.S., B.C., C.H.; formal analysis and data curation, A.R.R., A.J.B. E.J.V., E.B.-F., A.R.-I., G.A.; visualization, A.R.R., A.J.B., G.A., L.V.S., B.C., C.H.; writing—original draft preparation, A.R.R., A.J.B., E.B.-F., E.J.V.; writing—review and editing, all authors; funding acquisition A.R.R., S.G., V.D., P.C., N.M, F.V.; all authors have read and agreed to the published version of the manuscript.

**Competing interests:** The authors declare no conflict of interest. The funders had no role in the design of the study; in the collection, analyses, or interpretation of data; in the writing of the manuscript, or in the decision to publish the results.

**Data and materials availability:** All data used for the study is included in this paper. Materials used in the analysis are available upon request and depending on material availability.

## REFERENCES


Abouchami, W., Galer, S.J.G., Hofmann, A.W., 2000. High precision lead isotope systematics of lavas from the Hawaiian Scientific Drilling Project. Chemical Geology 169, 187–209. https://doi.org/10.1016/S0009-2541(00)00328-4

Artioli, G., Angelini, I., Nimis, P., Villa, I.M., 2016. A lead-isotope database of copper ores from the Southeastern Alps: a tool for the investigation of prehistoric copper metallurgy. Journal of Archaeological Science 75, 27–39. https://doi.org/10.1016/j.jas.2016.09.005

Baragona, A.J., Rodler, A.S., Bauerová, P., 2022. Imperial Styles, Frontier Solutions: Roman wall painting technology in the province of Noricum. In: Proceedings of the 6th Historic Mortars Conference, HMC2022 University of Ljubljana, SL. RILEM Sarl, France

Baxter, D.C., Rodushkin, I., Engström, E., Malinovsky, D., 2006. Revised exponential model for mass bias correction using an internal standard for isotope abundance ratio measurements by multi-collector inductively coupled plasma mass spectrometry. Journal of Analytical Atomic Spectrometry, 21, 427–430. https://doi.org/10.1039/B517457K

Beck, L.Y., 2005. De Materia Medica. Olms-Weidmann: Hildesheim.

Becker, H. 2021. Color Technology and Trade. In: Biggam, C. and Wolf, K. and Wharton, D. (eds) Cultural History of Color, ed. Bloomsbury Publishing, London, 35-48.

Becker, H. 2022. Pigment nomenclature in the ancient Near East, Greece, and Rome. Journal of Archaeological and Anthropological Sciences 14:20. DOI: 10.1007/s12520-021-01394-1

Becker, H. Commerce in color: the mechanics of the Roman pigment trade. *forthcoming*

Begemann, F., Schmitt-Strecker, S., Pernicka, E., 2003. On the Composition and Provenance of Metal Finds from Beşiktepe (Troia). In: Wagner, G.A., Pernicka, E., Uerpmann, HP. (eds) Troia and the Troad. Natural Science in Archaeology. Springer, Berlin, Heidelberg. https://doi.org/10.1007/978-3-662-05308-9_11

Bergquist, B. A., Blum, J. D., 2007. Mass-dependent and-independent fractionation of Hg isotopes by photoreduction in aquatic systems. Science 318 (5849), 417.

Blum, J.D., Bergquist, B.A., 2007. Reporting of variations in the natural isotopic composition of mercury. Analytical and Bioanalytical Chemistry 388, 353–359. https://doi.org/10.1007/s00216-007-1236-9

Bolea-Fernandez, E., Rua-Ibarz, A., Krupp, E.M., Feldmann, J., Vanhaecke, F., 2019. High-precision isotopic analysis sheds new light on mercury metabolism in long-finned pilot whales (Globicephala melas). Sci Rep 9, 7262 (2019). https://doi.org/10.1038/s41598-019-43825-z

Bracci, S. Cantisiani, E., Falzone, F., Marano, M., Tomassini, P., 2021. Archaeometry and Roman Wall Painting: The Case of pre-Hadrianic Paintings in Ostia Antica. In: Cavalieri and Tomassini (ed.) Le peinture murale antique: méthodes et apports d'une approche technique Actes du colloque international. Louvain la Neuve 21 April 2017 Edizioni Quasar

Çakmakoğlu, A., Bilgin, Z.R., 2006. Pre-Neogene Stratigraphy of The Karaburun Peninsula (W of İzmir Turkey). Bulletin of The Mineral Research and Exploration 132, 33–61.

Çakmakoğlu, B., Göktaş, F., Demirhan, M., Helvacı, C., 2013. Investigation of Stratigraphy, Sedimentology and Economical Usage of the Clays from the Northern Part of the Karaburun Peninsula. Geological Bulletin of Turkey 56(1), 39–58.

Chen, D., Ren, D., Deng, C., Tian, Z., Yin, R., 2022. Mercury loss and isotope fractionation during high-pressure and high-temperature processing of sediments: Implications for the behaviors of mercury during metamorphism. Geochimica et Cosmochimica Acta 334, 231–240. https://doi.org/10.1016/j.gca.2022.08.010

Cooke, C.A., Hintelmann, H., Ague, J.J., Burger, R., Biester, H., Sachs, J.P., Engstrom, D.R., 2013. Use and legacy of mercury in the Andes. Environmental Science & Technology 47, 4181−4188. https://doi.org/10.1021/es3048027

Delile, H., Blichert-Toft, J., Goiran, J.P., Stock, F., Arnaud-Godet, F., Bravard, J.P., Brückner, H., Albarède, F., 2015. Demise of a harbor: A geochemical chronicle from Ephesus. Journal of Archaeological Science 53, 202-213. https://doi.org/10.1016/j.jas.2014.10.002

Emslie, S.D., Brasso, R., Patterson, W.P., Valera, A.C., McKenzie, A., Silva, A.M., Gleason, J.D., Blum, J.D., 2015. Chronic mercury exposure in Late Neolithic/Chalcolithic populations in Portugal from the cultural use of cinnabar. Scientific Reports 5, 14679. DOI: 10.1038/srep14679

Esposito, D., 2014. La pittura di Ercolano. Studi della Soprintendenza Archeologica di Pompeii 33. Rome: "L'Erma" di Bretschneider

Esposito, D., 2017. The Economics of Pompeian Painting. In: Flohr, M. and Wilson, A. (eds.), The Economy of Pompeii (pp. 263-289). Oxford: Oxford University Press.

Faure, G., Mensing, T.M., 2005. Isotopes, Principles and Applications. 3rd ed. Hoboken Wiley.

Foss, C., Hanfmann, G.M.A., 1975. Reginal setting and urban development. In: Hanfmann, G.M.A., Jacobs, S.W. (eds.), Achraological Exploraiton of Sardis: A survey of Sardis and the major monuments outside the city walls. Harvard University Press, 17–34.

Fragnoli, P., Ugarković, M., Sterba, J.H., Sauer, R., 2022. Looking for Ephesian workshops: an integrated petrographic, geochemical, and chrono-typological approach to Late Hellenistic Ephesos lamps. Archaeological and Anthropological Sciences 14, 19. https://doi.org/10.1007/s12520-021-01419-9

Gale, N.H., Stos-Gale, Z.A., 1981. Lead and silver in the ancient Aegean. Scientific American 244(6), 176–192.

Gemici, Ü., 2008. Batı Anadolu'daki eski civa yataklarının çevre jeolojisi açısından değerlendirilmesi. In: Eşref Atabey (ed.) Uluslararası Katılımlı Tıbbi Jeoloji Sempozyumu Kitabı. 133–145.

Gemici, Ü., Oyman, T., 2003. The influence of the abandoned Kalecik Hg mine on water and stream sediments (Karaburun, Izmir, Turkey). Science of the Total Environment 312, 155–166. doi:10.1016/S0048-9697(03)00008-1

Gliozzo, E., 2021. Pigments — Mercury-based red (cinnabar-vermilion) and white (calomel) and their degradation products. Archaeological and Anthropological Sciences 13, 210. https://doi.org/10.1007/s12520-021-01402-4

Gökce, A., Bozkaya, G., 2007. Lead and sulfur isotopic studies of the barite–galena deposits in the Karalar area (Gazipaoa–Antalya), Southern Turkey. Journal of Asian Earth Sciences 30, 53–62. doi:10.1016/j.jseaes.2006.07.007

Gray, J.E., Pribil, M.J., Higueras, P.L., 2013. Mercury isotope fractionation during ore retorting in the Almadén mining district, Spain. Chemical Geology 357, 150–157. https://doi.org/10.1016/j.chemgeo.2013.08.036

Hauptmann, A., Schmitt-Strecker, S., Begemann, F., Palmieri, A.M., 2002. Chemical Composition and Lead Isotopy of Metal Objects from the "Royal" Tomb and Other Related Finds at Arslantepe, Eastern Anatolia. Paléorient 28, 43–69. http://www.jstor.org/stable/41496946

Helvacı, C. Ersoy, E.Y., Sözbilir, H., Erkül, F., Sümer, Ö., Uzel, B., 2009. Geochemistry and 40Ar/39Ar geochronology of Miocene volcanic rocks from the Karaburun Peninsula: Implications for amphibole-bearing lithospheric mantle source, Western Anatolia. Journal of Volcanology and Geothermal Research 185. 181–202.

Higueras, P., Munhá, J., Oyarzun, R., Tassinari, C.C.G., Ruiz, I.R., 2005. First lead isotopic data for cinnabar in the Almadén district (Spain): implications for the genesis of the mercury deposits. Mineralium Deposita 40, 115-122. https://doi.org/10.1007/s00126-005-0471-2

Hirao, Y., Enomoto, J., Tachikawa, H., 1995. Lead isotope ratios of copper, zinc and lead minerals in Turkey – in relation to the provenance study of artifacts. In: Prince Takahito Mikasa HIH (ed.) Essays on Ancient Anatolia and its surrounding civilisations. Harrassovitz Verlag, Wiesbaden, 89–114.

Hunt-Ortiz, M.A., Consuegra-Rodríguez, S., Díaz del Río-Español, P., Hurtado-Pérez, V.M., Montero-Ruiz, I., 2011. Neolithic and Chalcolithic – VI to III Millennia BC – use of cinnabar (HgS) in the

Iberian Peninsula: analytical identification and lead isotopic analysis for an early mineral exploitation of the Almadén (Ciudad Real, Spain) mining district. In: J. E. Ortiz, O. Puche, I. Rábano and L. F. Mazadiego (eds.) History of Research in Mineral Resources. Cuadernos del Museo Geominero, 13. Instituto Geológico y Minero de España, Madrid.

Keil, J., von Premerstein, A., 1914. Bericht über eine 3. Reise in Lydien und den angrenzenden Gebieten Ioniens, ausgeführt 1911 im Auftrage der Kaiserlichen Akademie der Wissenschaften (Wien 1914).

Klein, S., Domergue, C., Lahaye, Y., Brey, G.P., von Kaenel, H.-M., 2009. The lead and copper isotopic composition of copper ores from the Sierra Morena (Spain). J. Iber. Geol. 35, 59–68.

Klein, S., Lahaye, Y., Brey, G.P., von Kaenel, H.-M., 2004. The early Roman Imperial aes coinage II: tracing the copper sources by analysis of lead and copper isotopes – copper coins of Augustus and Tiberius. Archaeometry 46(3), 469–480.

Kostomitsopoulou Marketou, A., 2019. The pigment production site of the ancient agora of Kos (Greece): Revisiting the material evidence. THIASOS: Rivista di archeologia e architettura antica 8, 61–80.

Kostomitsopoulou Marketou, A., Andriulo, F., Steindal, C., Handberg, S., 2020. Egyptian blue pellets from the first century B.C.E workshop of Kos (Greece): Microanalytical investigation by Optical Microscopy, Scanning Electron Microscopy-X-ray Energy Dispersive Spectroscopy and Micro-Raman Spectroscopy. Minerals 10, 1063. https://doi.org/10.3390/min10121063

Kostomitsopoulou Marketou, A., Rodler-Rørbo, A., 2023. The Colourant Mapping Project: approaching the evidence of colourant production in the Aegean during the Hellenistic and Roman Period through Kea, Kos and Rhodes. Archaeological and Anthropological Sciences 15, 160. https://doi.org/10.1007/s12520-023-01849-7

Ladstätter, S., 2016. Hafen und Stadt von Ephesos in hellenistischer Zeit. Jahreshefte des Österreichischen Archäologischen Institutes in Wien 85, 233–272. ISSN 2309-1207

Lang-Auinger, C., 1996. Hanghaus 1 in Ephesos. Der Baubefund. Jahreshefte des Österreichischen Archäologischen Institutes in Wien VIII/3.

Lang-Auinger, C., Outschar, U., 1996. Aspekte zur Chronologie. In: Lang-Auinger, C. (ed.), Hanghaus 1 in Ephesos. Der Baubefund. Jahreshefte des Österreichischen Archäologischen Institutes in Wien VIII/3.

Lazzarini, L., Verità, M., 2015. First evidence for 1st century AD production of Egyptian blue frit in Roman Italy. Journal of Archaeological Science 53, 578–585.

Maras, A., Botticelli, M., Ballirano, P., 2013. Archaeometric investigations on cinnabar provenance and origin by X-ray powder diffraction: preliminary data. International Journal of Conservation Science 4, 685–692.

715 Mazzocchin, G. A., Baraldi, P., Barbante, C., 2008. Isotopic analysis of lead present in the cinnabar of
716 Roman wall paintings from the Xth Regio "(Venetia et Histria)" by ICP-MS. Talanta 74, 690–693.
717 https:// doi.org/10.1016/j.talanta.2007.06.048

718 Minami, T., Takeuchi, A., Imazu, S., Okuyama, M., Higashikage, Y., Mizuno, T., Okabayashi, K.,
719 Takahashi, K., 2021. Identification of source mine using sulfur, mercury, and lead isotope analyses
720 of vermilion used in three representative tombs from Kofun period in Japan. Journal of
721 Archaeological Science: Reports 37, 102970. https://doi.org/10.1016/j.jasrep.2021.102970

722 Ni, X., Yang, R., Yuan, W., Wang, X., Chen, J., Zhang, G., Li, D., Du, L., Gao, L., Luo, C., Zheng, L.,
723 Xu, H., 2022. New insight into the source of metals in Hg deposits at the southwestern margin of
724 the Yangtze Platform, China: Evidence from mercury stable isotope compositions. Ore Geology
725 Reviews 149, 105089. https://doi.org/10.1016/j.oregeorev.2022.105089

726 Nicholson, P.T., 2003. New excavations at a Ptolemaic-Roman faience factory at Memphis, Egypt.
727 Annales du 15e Congres de l'Association Internationale pour l'Histoire du Verre. AIHV 49–52.

728 Palero-Fernández, F.J., Martin-Izard, A., Prieto, M.Z., Mansilla-Plaza, L., 2015. Geological context and
729 plumbotectonic evolution of the giant Almadén Mercury Deposit. Ore Geology Reviews 64, 71–88.
730 https://doi.org/10.1016/j.oregeorev.2014.06.013

731 Pribil, M.J., Rimondi, V., Costagliola, P., Lattanzi, P., Rutherford, D.L., 2020. Assessing mercury
732 distribution using isotopic fractionation of mercury processes and sources adjacent and downstream
733 of a legacy mine district in Tuscany, Italy. Applied Geochemistry 117, 104600.
734 https://doi.org/10.1016/j.apgeochem.2020.104600

735 Prieto, G., Wright, V., Burger, R.L., Cooke, C.A., Zeballos-Velasquez, E.L., Watanave, A., Suchomel,
736 M.R., Suescun, L., 2015. The source, processing and use of red pigment based on hematite and
737 cinnabar at Gramalote, an early Initial Period (1500–1200 cal. B.C.) maritime community, north
738 coast of Peru. Journal of Archaeological Science: Reports 5, 45–60.
739 http://dx.doi.org/10.1016/j.jasrep.2015.10.026

740 Rodler, A. S., Artioli, G., Klein, S., Petschick, R., Fink-Jensen, P., Brøns, C., 2017. Provenancing ancient
741 pigments: Lead isotope analyses of the copper compound of Egyptian blue pigments from ancient
742 Mediterranean artifacts. Journal of Archaeological Science: Reports 16, 1–18. https://doi.
743 org/10.1016/j.jasrep.2017.09.008

744 Rodríguez, J, Montero-Ruiz, I, Hunt-Ortiz, M, García-Pavón, E., 2020. Cinnabar provenance of
745 Chalcolithic red pigments in the Iberian Peninsula: A lead isotope study. Geoarchaeology, 1–12.
746 https://doi.org/10.1002/gea.21810

747 Rua-Ibarz, A., Bolea-Fernandez, E., Maage, A., Frantzen, S., Sanden, M., Vanhaecke, F., 2019. Tracing
748 mercury pollution along the Norwegian Coast via elemental, speciation, and isotopic analysis of
749 liver and muscle tissue of deep-water marine fish (*Brosme brosme*). Environmental Science &
750 Technology 53, 1776–1785. https://doi.org/10.1021/acs.est.8b04706

Rua-Ibarz, A., Bolea-Fernandez, E., Maage, A., Frantzen, S., Valdersnes, S., Vanhaecke, F., 2016b. Assessment of Hg pollution released from a WWII submarine wreck (U-864) by Hg isotopic analysis of sediments and *Cancer pagurus* tissues. Environmental Science & Technology 50, 10361–10369. DOI: 10.1021/acs.est.6b02128

Rua-Ibarz, A., Bolea-Fernandez, E., Vanhaecke, F., 2016a. An in-depth evaluation of accuracy and precision in Hg isotopic analysis via pneumatic nebulization and cold vapor generation multi-collector ICP-mass spectrometry. Analytical and Bioanalytical Chemistry, 408, 417−429. DOI:10.1007/s00216-015-9131-2

Salvadori, M., Sbrolli, C., 2021. Wall paintings through the ages: the roman period – Republic and early Empire. Archaeological and Anthropological Sciences 13, 187. https://doi.org/10.1007/s12520-021-01411-3

Sayre, E.V., Joel, E.C., Blackman, M.J., Yener, K.A., Özbal, H., 2001. Stable lead isotope studies of Black Sea Anatolian ore sources and related Bronze age and Phrygian artefacts from nearby archaeological sites. Appendix: new Central Taurus ore data. Archaeometry 43, 77–115.

Scherrer, P., Trinkl, E., 2006. Die Tetragonos Agora in Ephesos. Grabungsergebnisse von archaischer bis in byzantinische Zeit – Ein Überblick Befunde und Funde klassischer Zeit. Jahreshefte des Österreichischen Archäologischen Institutes in Wien XIII/2.

Schmeisser, C., 1906. Bodenschätze und Bergbau Kleinasiens. Zeitschrift für praktische Geologie XIV, 6, 186-196.

Smith, R.S., Wiederhold, J.G., Jew, A.D., Brown Jr., G.E., Bourdon, B., Kretzschmar, R., 2014. Small-scale studies of roasted ore waste reveal extreme ranges of stable mercury isotope signatures. Geochimica et Cosmochimica Acta 137, 1–17. https://doi.org/10.1016/j.gca.2014.03.037

Spangenberg, J.E., Lavrič, J.V., Meisser, N., Serneels, V., 2010. Sulfur isotope analysis of cinnabar from Roman wall paintings by elemental analysis/isotope ratio mass spectrometry – tracking the origin of archaeological red pigments and their authenticity. Rapid communications in Mass Spectrometry 24(19), 2812-2816. https://doi.org/10.1002/rcm.4705

Stephens, J.A., Ducea, M.N., Killick, D.J., Ruiz, J., 2021. Use of non-traditional heavy stable isotopes in archaeological research. Journal of Archaeological Science 127, 105334. https://doi.org/10.1016/j.jas.2021.105334

Stetson, S.J., Gray, J.E., Wanty, R.B., Macalady, D.L., 2009. Isotopic Variability of Mercury in Ore, Mine-Waste Calcine, and Leachates of Mine-Waste Calcine from Areas Mined for Mercury. Environmental Science and Technology 43, 7331–7336. *https://doi.org/10.1021/es9006993*

Stos-Gale, Z.A., Gale, N.H., 2009. Metal provenancing using isotopes and the Oxford archaeological lead isotope database (OXALID). Archaeological and Anthropological Sciences 1, 195–213. https://doi.org/10.1007/s12520-009-0011-6

Tezgör, D.K., 2022. From the miltos / sinopis of ancient Sinope to the Yoşa of Modern Cappadocia. Adalya 25, 45–69. http://orcid.org/0000-0002-5736-1822

Thür, H., 2005. Hanghaus 2 in Ephesos – die Wohneinheit 4. Jahreshefte des Österreichischen Archäologischen Institutes in Wien VIII/6.

Thür, H., Rathmayr, E., 2014. Hanghaus 2 in Ephesos – die Wohneinheit 6. Jahreshefte des Österreichischen Archäologischen Institutes in Wien VIII/9.

Tober, B., 2021. Ephesos – Palmyra – Noricum. Room-decoration as an international Code for living with images under the Roman imperial period. In: Thomas, R. (ed.), Local Styles or Common Pattern Books in Roman Wall Painting and Mosaics (Panel 3.22), Proceedings of the 19th International Congress of Classical Archaeology Cologne/Bonn 22 65-80 Heidelberg 22-26 May 2018

Tsantini, E., Minami, T., Takahashi, K., Ontiveros, M.Á.C., 2018. Analysis of sulphur isotopes to identify the origin of cinnabar in the Roman wall paintings from Badalona (Spain). Journal of Archaeological Science: Reports 18, 300-307. https://doi.org/10.1016/j.jasrep.2018.01.032

Vanderstraeten, A., Bonneville, S., Gili, S., de Jong, J., Debouge, W., Claeys, P., Mattielli, N., 2020. First multi-isotopic (Pb-Nd-Sr-Zn-Cu-Fe) characterisation of dust reference materials (ATD and BCR-723): A multi-column chromatographic method optimised to trace mineral and anthropogenic dust sources. Geostandards and Geoanalytical Research 44, 307–329. doi:10.1111/ggr.12320

Wagner, G.A., Pernicka, E., Seeliger, T.C., Öztunali, Ö., Baranyi, I., Begemann, F., Schmitt-Strecker, S., 1985. Geologische Untersuchungen zur frühen Metallugie in NW-Anatolien. Bulletin of the Mineral Research and Exploration Inst. Turkey 101/102, 45–81.

Weis, D., Kieffer, B., Maerschalk, C., Barling, J., de Jong, J., Williams, G., Hanano, D., Pretorius, W., Mattielli, N., Scoates, J., Goolaerts, A., Friedman, R., Mahoney, J., 2006. High-precision isotopic characterization of USGS reference materials by TIMS and MC-ICP-MS: Isotopic study of USGS reference materials. Geochemistry, Geophysics, Geosystems, 7(8), Q08006, doi:10.1029/2006GC001283.

Weis, D., Kieffer, B., Maerschalk, C., Pretorius, W., Barling, J., 2005. High-precision Pb-Sr-Nd-Hf isotopic characterization of USGS BHVO-1 and BHVO-2 reference materials. Geochemistry, Geophysics, Geosystems, 6, Q02002, doi:10.1029/2004GC000852.

Willett, F., Sayre, E.V., 2006. Lead isotope in West African copper alloys. Journal of African Archaeology 4, 55–90.

Yener, K.A., Sayre, E.V., Joel, E.C., Özbal, H., Barnes, I.L., Brill, R.H., 1991. Stable lead isotope studies of Central Taurus ore sources and related artifacts from Eastern Mediterranean Chalcolithic and Bronze age sites. Journal of Archaeological Science 18, 541–577.

Yesares, L., Sáez, R., De Almodóvar, G.R., Nieto, J.M., Gómez, G., Ovejero, G., 2017. Mineralogical evolution of the Las Cruces gossan cap (Iberian Pyrite Belt): From subaerial to underground conditions. Ore Geology Reviews 80, 377–405. https://doi.org/10.1016/j.oregeorev.2016.05.018

Yin, R., Feng, X., Hurley, J.P., Krabbenhoft, D.P., Lepak, R.F., Hu, R., Zhang, Q., Li, Z., and Bi, X., 2016. Mercury Isotopes as Proxies to Identify Sources and Environmental Impacts of Mercury in Sphalerites. Scientific Reports 6, 18686. https://doi.org/10.1038/srep18686

Yin, R., Feng, X., Wang, J., Li, P., Liu, J., Zhang, Y., Chen, J., Zhen, L., Hu, T., 2013. Mercury speciation and mercury isotope fractionation during ore roasting process and their implication to source identification of downstream sediment in the Wanshan mercury mining area, SW China. Chemical Geology 336, 72–79. https://doi.org/10.1016/j.chemgeo.2012.04.030

Yıldız, M., 1967. Mercury: Maden Tetkik ve Arama Enst. (MTA) Bull, 68.

Yıldız, M., Bailey, E.H., 1978. Mercury deposits in Turkey. Geological Survey Bulletin 1456, 1–79.

Zabrana, L., 2022. Das Artemision von Ephesos als Wirtschaftszentrum in römischer Zeit. Neue archäologische Forschungen des Österreichischen Archäologischen Institutes. In: Alkier, S. (ed) Konstellationen antiker Tempelwirtschaft, Beyond Historicism – New Testament Studies Today Vol. 1.

Zimmermann, G.A., 1874. Ephesos im ersten christlichen Jahrhundert (Jena 1874).

Zimmermann, N., 2005. Wandmalerei. In: Thür, H. (ed.), Hanghaus 2 in Ephesos – die Wohneinheit 4. Jahreshefte des Österreichischen Archäologischen Institutes in Wien VIII/6.

Zimmermann, N., 2014. Wandmalerei. In: Thür, H., Rathmayr, E. (eds.), Hanghaus 2 in Ephesos – die Wohneinheit 6. Jahreshefte des Österreichischen Archäologischen Institutes in Wien VIII/9.

Zimmermann, N., 2016a. Wandmalerei. In: Rathmayr, E. (ed.), Hanghaus 2 in Ephesos – die Wohneinheit 7. Jahreshefte des Österreichischen Archäologischen Institutes in Wien VIII/10.

Zimmermann, N., 2016b. Die Entwicklung der Wandmalerei in Kleinasien von der griechischen bis zur römischen Zeit am Beispiel von Ephesos. In: Dubois, Y., Niffeler, U. (eds.), Pictores per provincias II – Status Quaestionis. Actes du 13e Colloque de l'Association Internationale pour la Peinture Murale Antique (AIPMA), Université de Lausanne, 12–16 septembre 2016.

**Table 1.** Cinnabar grain size diameter, average particle size and intergranular spacing for the Ephesian wall painting fragments analyzed

| Painting technique | Sample ID | Site | Cinnabar grain size diameter | | | | | | Average particle size (µm) | Average intergranular space (µm) |
|---|---|---|---|---|---|---|---|---|---|---|
| | | | <1 µm (%) | 1-2 µm (%) | 2-3 µm (%) | 3-5 µm (%) | 5-10 µm (%) | >10 µm (%) | | |
| **1–Agora** | EPHCIN-28 | Agora | n.d. | n.d. | 1.00 | 23.0 | 56.0 | 20.0 | 8.25 | 4.50 |
| **2–TH1** | EPHCIN-24 | Terrace House 1 | 3.00 | 19.0 | 14.0 | 24.0 | 32.0 | 8.00 | 4.70 | 3.10 |
| **3–TH2A** | EPHCIN-06 | Terrace House 2, Room 36 | n.d. | 43.0 | 15.0 | 20.0 | 31.0 | 6.00 | 3.50 | 7.00 |
| **4–TH2B** | EPHCIN-25 | Room 45, Taberna adjacent to living unit 7 of Terrace House 2 | 3.00 | 9.00 | 12.0 | 18.0 | 44.0 | 15.0 | 6.70 | 5.00 |
| | | Average across samples | 1.50 | 17.8 | 10.5 | 21.3 | 40.8 | 12.3 | 5.79 | 4.90 |

**Notes:** Tabular display of the information given in Fig. 1, with the additional information of the average cinnabar intergranular space; this is based on the analysis of all cross-sectioned samples even though only the four shown in Fig. 1 are mentioned here as examples.

**Table 2.** Isotope ratio data for cinnabar samples from Ephesian wall painting fragments and cinnabar ore from the Karaburun Peninsula, Turkey

| | Sample ID | $^{206}Pb/^{204}Pb$ | $^{207}Pb/^{204}Pb$ | $^{208}Pb/^{204}Pb$ | $^{207}Pb/^{206}Pb$ | $^{208}Pb/^{206}Pb$ | $\Delta^{199}Hg$<br>*$\delta^{199}Hg$* | $\Delta^{200}Hg$<br>*$\delta^{200}Hg$* | $\Delta^{201}Hg$<br>*$\delta^{201}Hg$* | *$\delta^{202}Hg$* |
|---|---|---|---|---|---|---|---|---|---|---|
| Cinnabar, Ephesian wall painting fragments | EPHCIN-02[1] | 18.711 ± 0.001 | 15.684 ± 0.001 | 38.880 ± 0.002 | 0.83822 ± 0.00001 | 2.07791 ± 0.00004 | | | | |
| | EPHCIN-06[1] | 18.771 ± 0.001 | 15.683 ± 0.001 | 38.819 ± 0.002 | 0.83549 ± 0.00002 | 2.06797 ± 0.00004 | -0.13 ± 0.04<br>*0.15 ± 0.05* | -0.03 ± 0.06<br>*0.54 ± 0.06* | -0.10 ± 0.05<br>*0.75 ± 0.05* | *1.13 ± 0.05* |
| | EPHCIN-13[1] | 18.686 ± 0.001 | 15.671 ± 0.001 | 38.818 ± 0.002 | 0.83865 ± 0.00001 | 2.07744 ± 0.00003 | -0.09 ± 0.06<br>*0.07 ± 0.08* | 0.01 ± 0.07<br>*0.32 ± 0.11* | -0.13 ± 0.06<br>*0.34 ± 0.10* | *0.62 ± 0.10* |
| | EPHCIN-14[1] | 18.688 ± 0.001 | 15.671 ± 0.001 | 38.817 ± 0.002 | 0.83853 ± 0.00001 | 2.07707 ± 0.00004 | | | | |
| | EPHCIN-17[2]* | 18.818 ± 0.001 | 15.684 ± 0.001 | 38.864 ± 0.002 | 0.83348 ± 0.00002 | 2.06529 ± 0.00004 | | | | |
| | EPHCIN-19[1]* | 18.624 ± 0.001 | 15.672 ± 0.001 | 38.824 ± 0.002 | 0.84150 ± 0.00002 | 2.08457 ± 0.00004 | | | | |
| | EPHCIN-20[1]* | 18.613 ± 0.001 | 15.670 ± 0.001 | 38.805 ± 0.002 | 0.84183 ± 0.00002 | 2.08479 ± 0.00005 | -0.13 ± 0.04<br>*0.07 ± 0.03* | 0.05 ± 0.05<br>*0.45 ± 0.05* | -0.16 ± 0.07<br>*0.43 ± 0.04* | *0.79 ± 0.08* |
| | EPHCIN-21[3] | 18.756 ± 0.001 | 15.681 ± 0.001 | 38.933 ± 0.003 | 0.83603 ± 0.00001 | 2.07582 ± 0.00005 | | | | |
| | EPHCIN-23[4] | 18.385 ± 0.001 | 15.648 ± 0.001 | 38.474 ± 0.002 | 0.85113 ± 0.00001 | 2.09270 ± 0.00004 | | | | |
| | EPHCIN-24[4] | 18.245 ± 0.001 | 15.635 ± 0.001 | 38.266 ± 0.002 | 0.85695 ± 0.00003 | 2.09733 ± 0.00006 | -0.11 ± 0.05<br>*0.08 ± 0.05* | -0.02 ± 0.04<br>*0.36 ± 0.04* | -0.11 ± 0.07<br>*0.46 ± 0.08* | *0.76 ± 0.05* |
| | EPHCIN-25[5] | 18.526 ± 0.001 | 15.656 ± 0.001 | 38.559 ± 0.002 | 0.84507 ± 0.00001 | 2.08135 ± 0.00004 | -0.40 ± 0.06<br>*-0.13 ± 0.07* | -0.02 ± 0.04<br>*0.52 ± 0.06* | -0.33 ± 0.09<br>*0.48 ± 0.09* | *1.07 ± 0.07* |
| | EPHCIN-26[6] | 18.784 ± 0.001 | 15.685± 0.001 | 38.958 ± 0.002 | 0.83504 ± 0.00002 | 2.07408 ± 0.00003 | -0.31 ± 0.03<br>*-0.15 ± 0.04* | -0.04 ± 0.05<br>*0.29 ± 0.04* | -0.21 ± 0.08<br>*0.29 ± 0.04* | *0.66 ± 0.08* |
| | EPHCIN-27[6]* | 18.768 ± 0.001 | 15.683 ± 0.001 | 38.942 ± 0.002 | 0.83563 ± 0.00001 | 2.07490 ± 0.00004 | | | | |
| | EPHCIN-28[6] | 18.760 ± 0.001 | 15.682 ± 0.001 | 38.907 ± 0.002 | 0.83591 ± 0.00001 | 2.07389 ± 0.00004 | | | | |
| Karaburun cinnabar ore | EPHCINO-03$_D$ | 19.034 ± 0.001 | 15.704 ± 0.001 | 38.986 ± 0.002 | 0.82501 ± 0.00001 | 2.04821 ± 0.00003 | -0.05 ± 0.03<br>*-0.04 ± 0.04* | 0.01 ± 0.05<br>*0.04 ± 0.05* | -0.07 ± 0.03<br>*-0.03 ± 0.06* | *0.05 ± 0.06* |
| | EPHCINO-04$_D$* | 18.963 ± 0.001 | 15.701 ± 0.001 | 38.953 ± 0.002 | 0.82800 ± 0.00001 | 2.05414 ± 0.00004 | | | | |
| | EPHCINO-05$_K$* | 19.202 ± 0.001 | 15.706 ± 0.001 | 38.623 ± 0.002 | 0.81800 ± 0.00001 | 2.01149 ± 0.00004 | | | | |
| | EPHCINO-08$_K$ | 19.464 ± 0.001 | 15.721 ± 0.001 | 38.735 ± 0.002 | 0.80772 ± 0.00001 | 1.99012 ± 0.00004 | -0.15 ± 0.11<br>*-0.20 ± 0.13* | 0.00 ± 0.07<br>*-0.12 ± 0.10* | -0.11 ± 0.05<br>*-0.29 ± 0.08* | *-0.23 ± 0.08* |
| | EPHCINO-11$_K$ | 19.332 ± 0.001 | 15.721 ± 0.001 | 38.746 ± 0.002 | 0.81320 ± 0.00001 | 2.00423 ± 0.00004 | -0.22 ± 0.04<br>*-0.19 ± 0.03* | -0.02 ± 0.05<br>*0.04 ± 0.06* | 0.02 ± 0.12<br>*0.11 ± 0.15* | *0.12 ± 0.06* |
| | EPHCINO-12$_K$ | 19.130 ± 0.001 | 15.710 ± 0.001 | 38.692 ± 0.002 | 0.82125 ± 0.00001 | 2.02261 ± 0.00003 | | | | |
| | BHVO-2 | 18.453 ± 0.001 | 15.669 ± 0.001 | 38.626 ± 0.003 | 0.84915 ± 0.00002 | 2.09321 ± 0.00005 | -0.15 ± 0.06<br>*0.05 ± 0.06* | 0.03 ± 0.03<br>*0.42 ± 0.04* | -0.21 ± 0.06<br>*0.38 ± 0.06* | *0.79 ± 0.09* |
| | BHVO-2** | 18.62 ± 0.05 | 15.53 ± 0.05 | 38.21 ± 0.04 | | | | | | |

**Notes:** Pb and Hg isotope ratios (±2SE) for samples of Terrace House 2: [1] Living unit 6 (Room 36a), [2] Living unit 3 (Room 12), [3] Living unit 4 (Room 21), [5] Room 45 (Taberna), Terrace House 1: [4] Taberna IV, and the [6] Agora; Karaburun ores EPHCINO-03$_D$ and -04$_D$, and EPHCINO-05$_K$, -08$_K$, -11$_K$ and -12$_K$ are from the Dikencik and Kalecik deposits, resp. (Fig. 1); *mean values (n=2); ** Pb isotope ratio data for reference material BHVO-2 (±2SD; Weis et al., 2005)

**Table 3:** Painting technique and cinnabar source groupings with the archaeological context of the Ephesian wall painting fragments analyzed

| | **SEM micrograph** | **Cross section** | **Painting technique**<br>Sample ID | **Geochemistry-based groupings**<br>LID – Pb isotope ratio data<br>HgID – Hg isotope ratio data | **Archaeological context** |
|---|---|---|---|---|---|
| **Cinnabar layer with little to no ochre admixing** | Thin, compact cinnabar layer on red ochre | Thin, compact cinnabar only layer on ochre, rough intonaco | **1–Agora**<br>EPHCIN-26, -27, -28 | All Agora samples have similar LID; all within the range of TH2 samples, overlapping with Turkish / Balkan references (Fig. 2); EPHCIN-26 (and -25): perhaps different heat treatment compared to other samples (Fig. 3A) | Tetragonos Agora<br>Southern portal<br>Part of the Roman agora, 1st–3rd c. CE [1] |
| | Relatively dense cinnabar layer with little to no ochre admixing | Cinnabar mixed with some ochre, on yellow and red ochre layer | **2–TH1**<br>EPHCIN-23, -24 | Different from other samples (Fig. 3); mixed signal or unknown source? But similar heat processing as TH2 samples (Fig. 3A) | Terrace House 1 (TH1), Taberna IV<br>Levelling layer with wall painting fragments dated to 1st c. CE [2]; samples likely from a reconstruction phase (~17–140 CE) [3] |
| | | Thick cinnabar only on intonaco layer tinted with red ochre | **4–TH2B**<br>EPHCIN-25 | Different from other samples, but better overlap with Balkan reference LID (Fig. 3); different heat treatment (Fig. 3A) | Terrace House 2 (TH2), Room 45<br>Taberna adjacent to and at times part of Living Unit 7; up to eight painting phases *in situ* and dated between the 1st–3rd c. CE [4] |
| **Cinnabar mixed with ochre** | Thin cinnabar layer with larger spacing of grains (due to ochre admixing) | *Cinnabar mixed with ochre* over red ochre | **3–TH2A**<br>EPHCIN-02, -06, -13, -14, -19, -20 | Larger cluster of TH2 samples, overlapping with Turkish and Balkan reference LID (Fig. 2); similar material heat processing as TH1 sample (Fig. 3A) | TH2, Living Unit 6, Room 36<br>Living area of ~650 m$^2$; Room 36 is part of representative rooms, cinnabar pigment was likely used for the upper floor and pertains to an earlier painting phase (**I-III**) [5] * |
| | | | EPHCIN-21 | | TH2, Living Unit 4, Room 21<br>Living area of ~460–360 m$^2$, Room 21 is the Peristyle (~160 m$^2$) [6]; the sampled wall painting fragment likely pertains to the Peristyle upper floor of Room 21, dated to building phase **II** [7] * |
| | | | EPHCIN-17 | | TH2, Living Unit 3, Room 12<br>Living area of ~260 m$^2$, Room 12 is the Muse room, wall paintings pertain to building phase **IV** [8] |

**Notes:** Scherrer and Trinkl (2006: 11); [2] Lang-Auinger (1996: 121-123); [3] Lang-Auinger and Outschar (1996); [4] Zimmermann (2016a: 731); [5] Zimmermann (2014: 287, 309, 323); [6] Thür (2005: 51); Zimmermann (2005: 106); [7] Zimmermann (2005: 110, 128-129); [8] Zimmermann (2016b: 82); * building phases in Terrace House 2 are grouped as **I** until mid-1st c. CE, **II** ~120 CE, **III** mid-2nd c. CE, and **IV** early 3rd c. CE (Zimmermann, 2005).

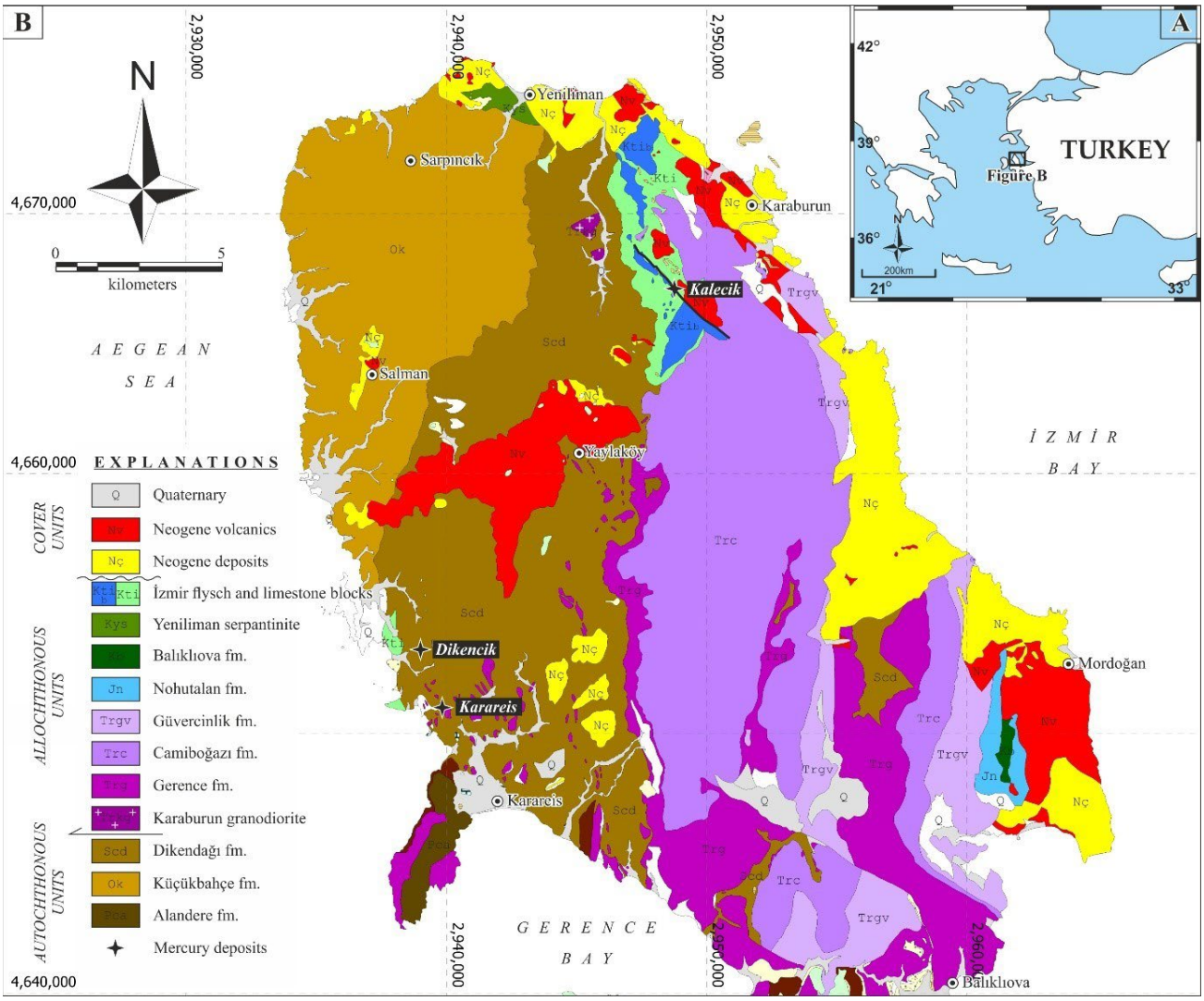


**Figure 1.** Geological map of the northern part of the Karaburun Peninsula (simplified from Çakmakoğlu and Bilgin, 2006) with the sampling sites at the deposits of Karareis, Dikencik and Kalecik indicated with black stars; samples from the Dikencik and Kalecik deposits were included in this study.

(2-column fitting image)

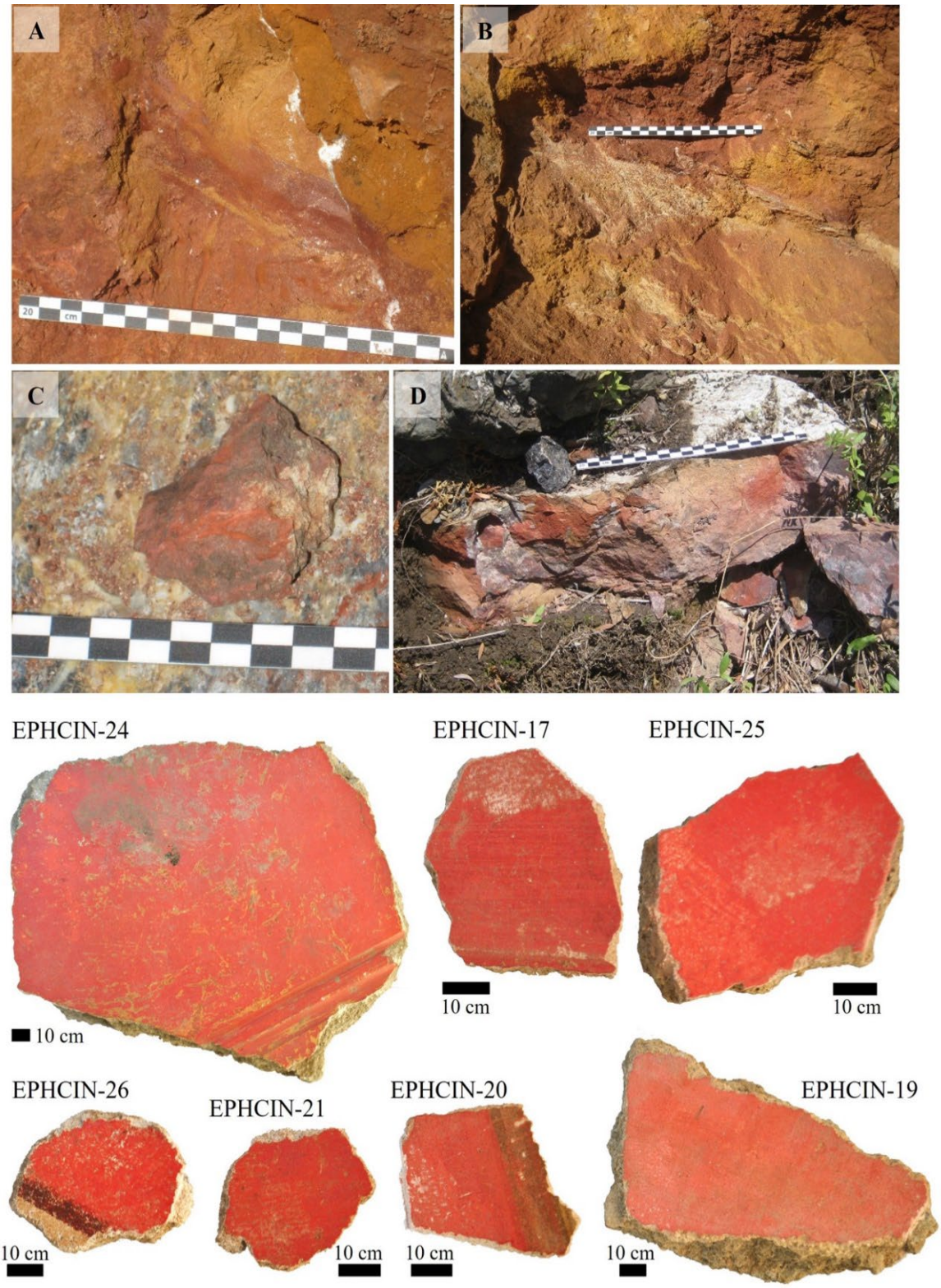


**Figure 2.** Field photographs at sites where cinnabar was collected at Kalecik (**A-B**) and Dikencik (**C-D**) (Photos: L.V. Sørensen, B. Çakmakoğlu, C. Helvacı), and examples of wall painting fragments where samples were collected (Photos: A. Rodler-Rørbo) (2-column fitting image)

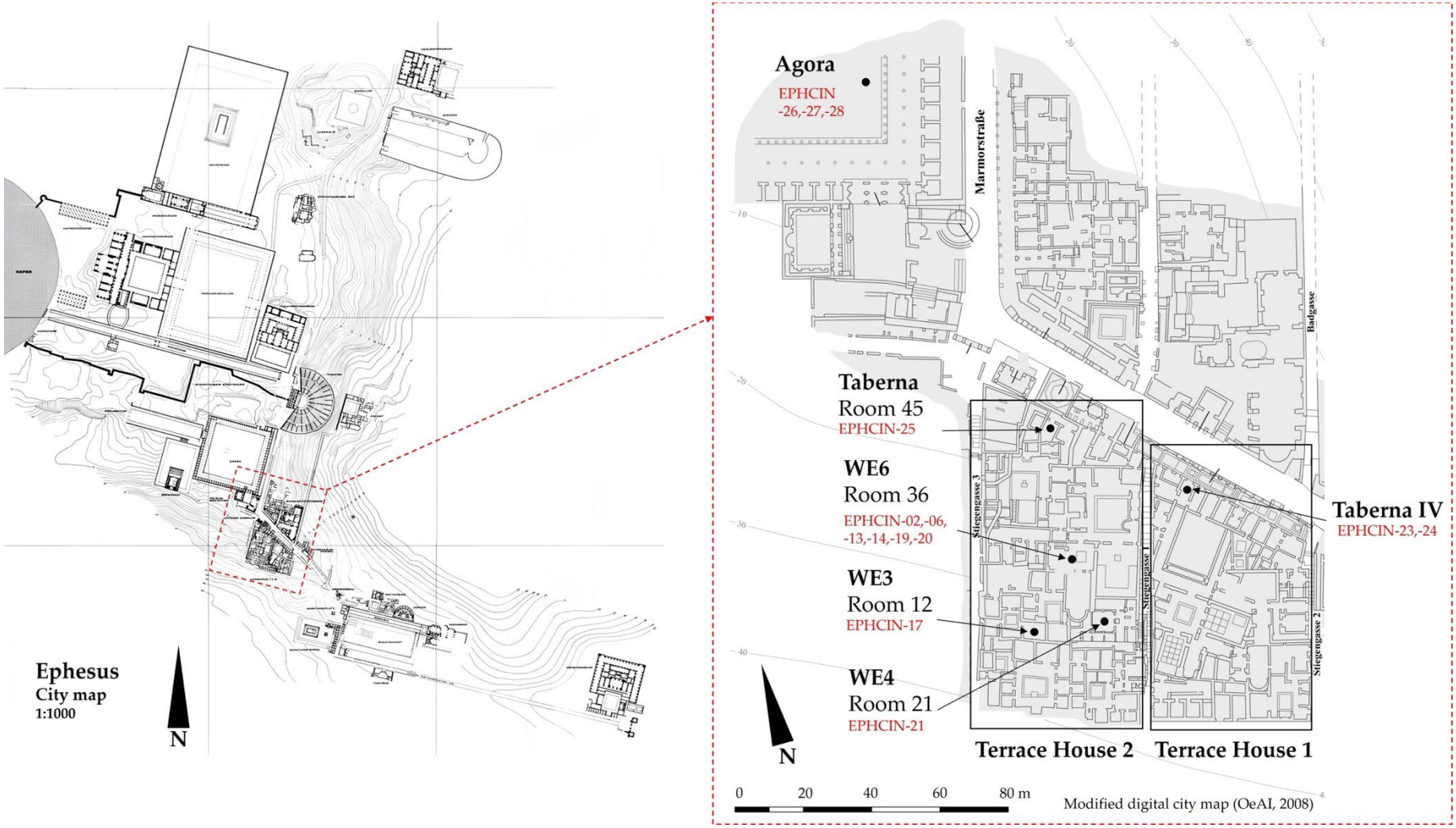


**Figure 3.** Site and sample location maps, incl. the Agora, Terrace House 1 and 2, with the collected samples (EPHCIN-#, see Tab. 3)

(2-column fitting image)

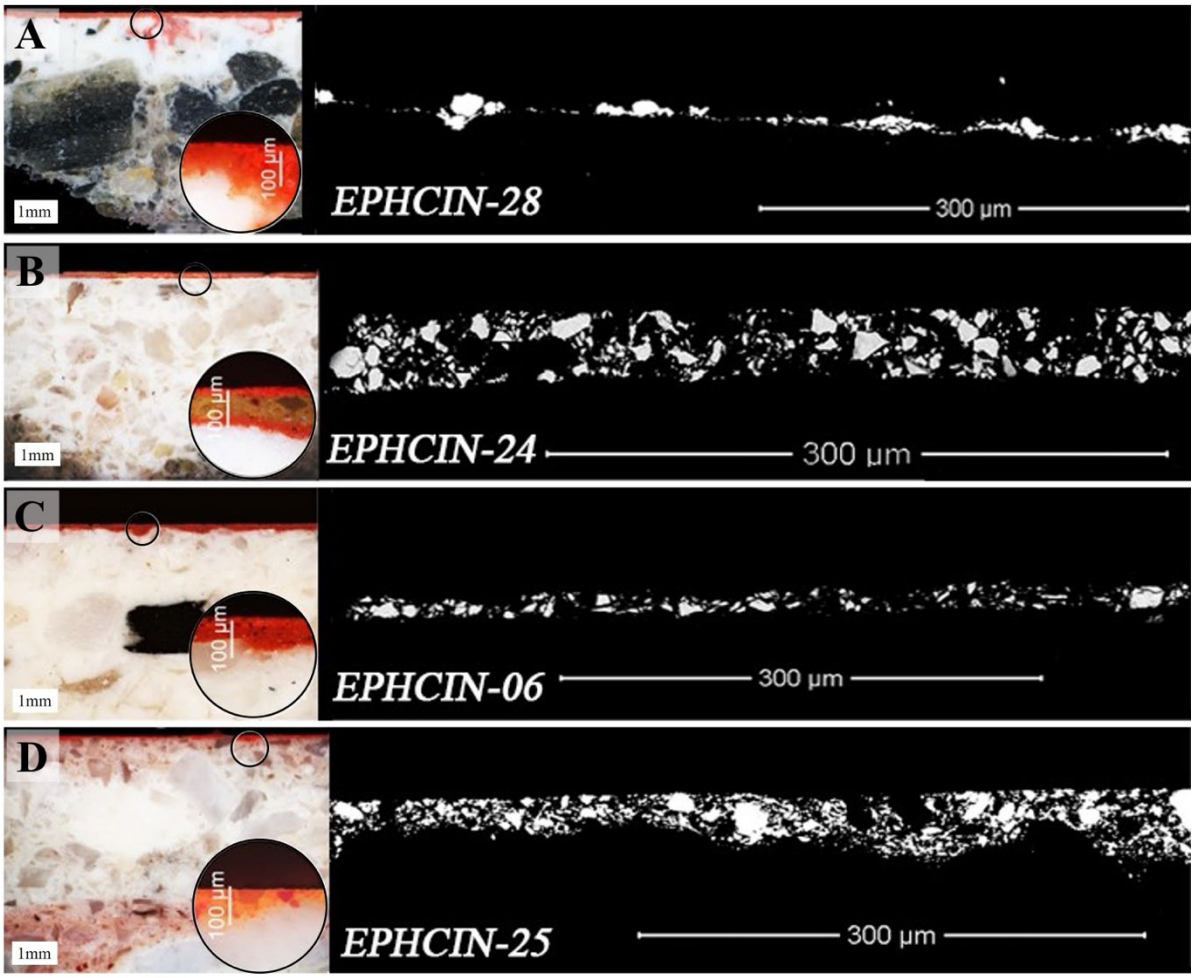


**Figure 4.** *Left*, Cross-section images of four wall painting fragments from the subject area displaying different painting techniques with corresponding over-exposed SEM micrographs showing grain size distribution of cinnabar only (ochre not visible) (Tab. 1)*, to the right.*: ***A)*** *Technique 1* – 'Agora' (sample EPHCIN-28): *left*, thin, compact cinnabar layer on ochre applied *a secco* without polishing, rough intonaco; *right*, thin, compact cinnabar layer over red ochre; ***B)*** *Technique 2* – 'TH1' (Terrace House 1, sample EPHCIN-24): *left*, cinnabar mixed with some ochre, over yellow ochre, red ochre; layers *right*, relatively dense cinnabar pigment layers with some ochre admixing; ***C)*** *Technique 3* – 'TH2A' (Terrace House 2, Room 36, sample EPHCIN-06): *left*, cinnabar mixed with ochre over red ochre; *right*, a thinner cinnabar layer displaying larger spacing of grains (attributable to ochre mixed with the cinnabar); ***D)*** *Technique 4* – 'TH2B' (Room 45, Taberna adjacent to Living Unit 7 of Terrace House 2, sample EPHCIN-25): *left*, thick cinnabar-only on an intonaco layer tinted with red ochre; *right*, the thick, dense layer of cinnabar pigment grains.

(2-column fitting image)

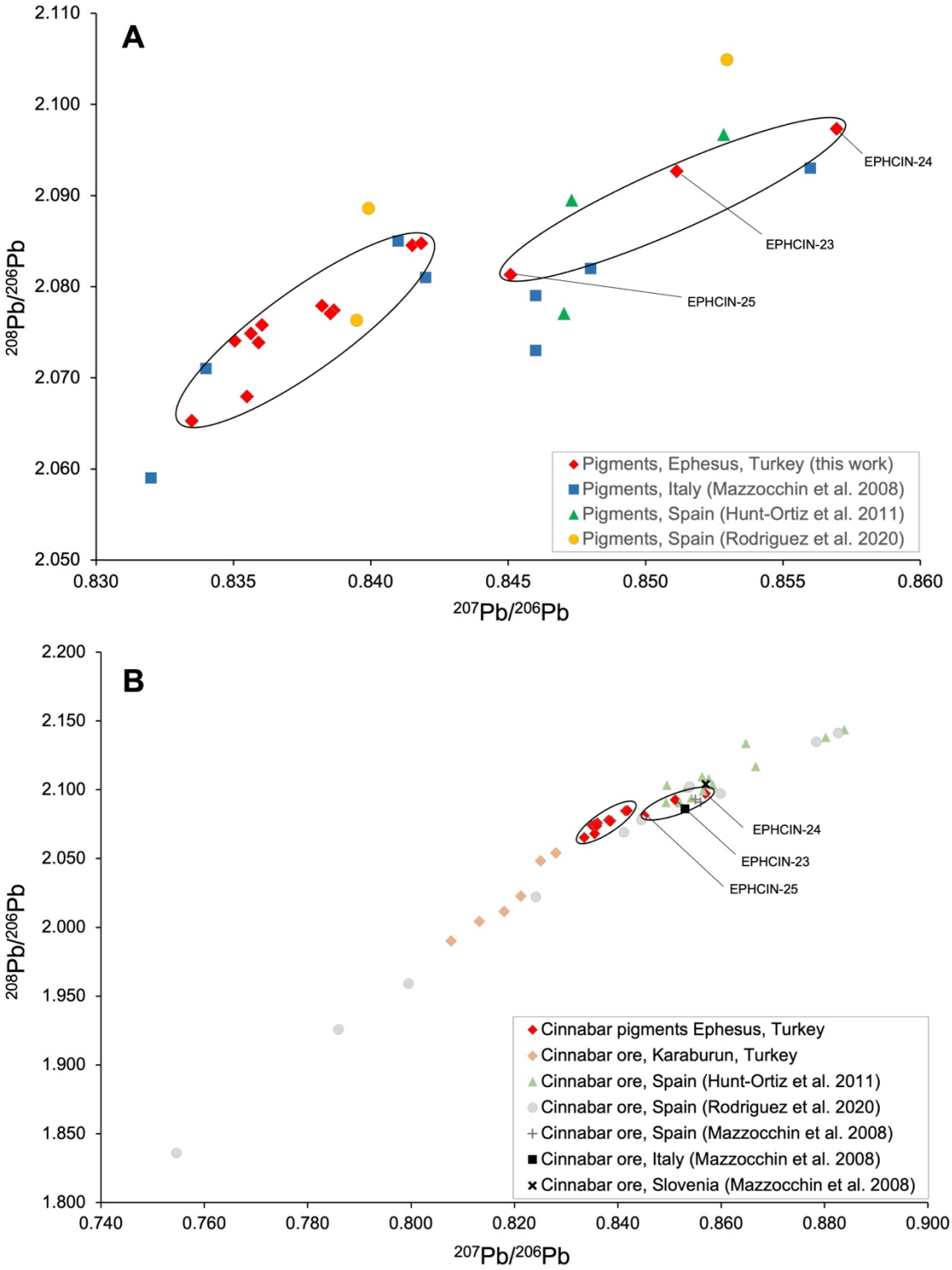


**Figure 5.** Pb isotope ratios of **A** cinnabar pigment samples from Ephesus (this work; ellipse: Terrace House 2 and Agora samples), Italy and Spain, and **B** cinnabar ore samples from Karaburun (Turkey), Spain, Italy, and Slovenia.
(2-column fitting image)

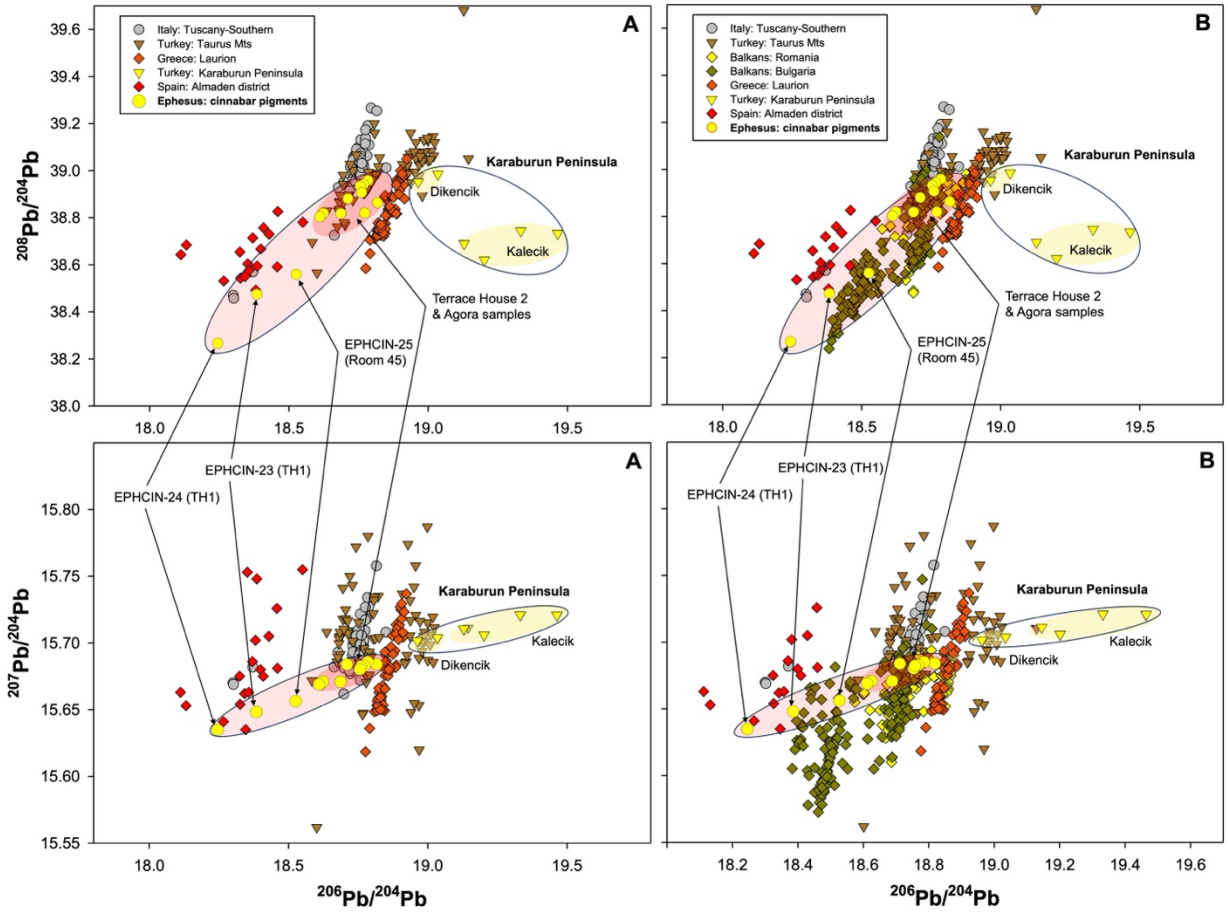


**Figure 6.** Pb isotope ratios for wall painting samples from Ephesus, ore samples from the Karaburun Peninsula and reference data for **A** Italy, Turkey, Greece, and Spain, **B** as well as with Balkan reference data from the AAcP database.

(2-column fitting image)

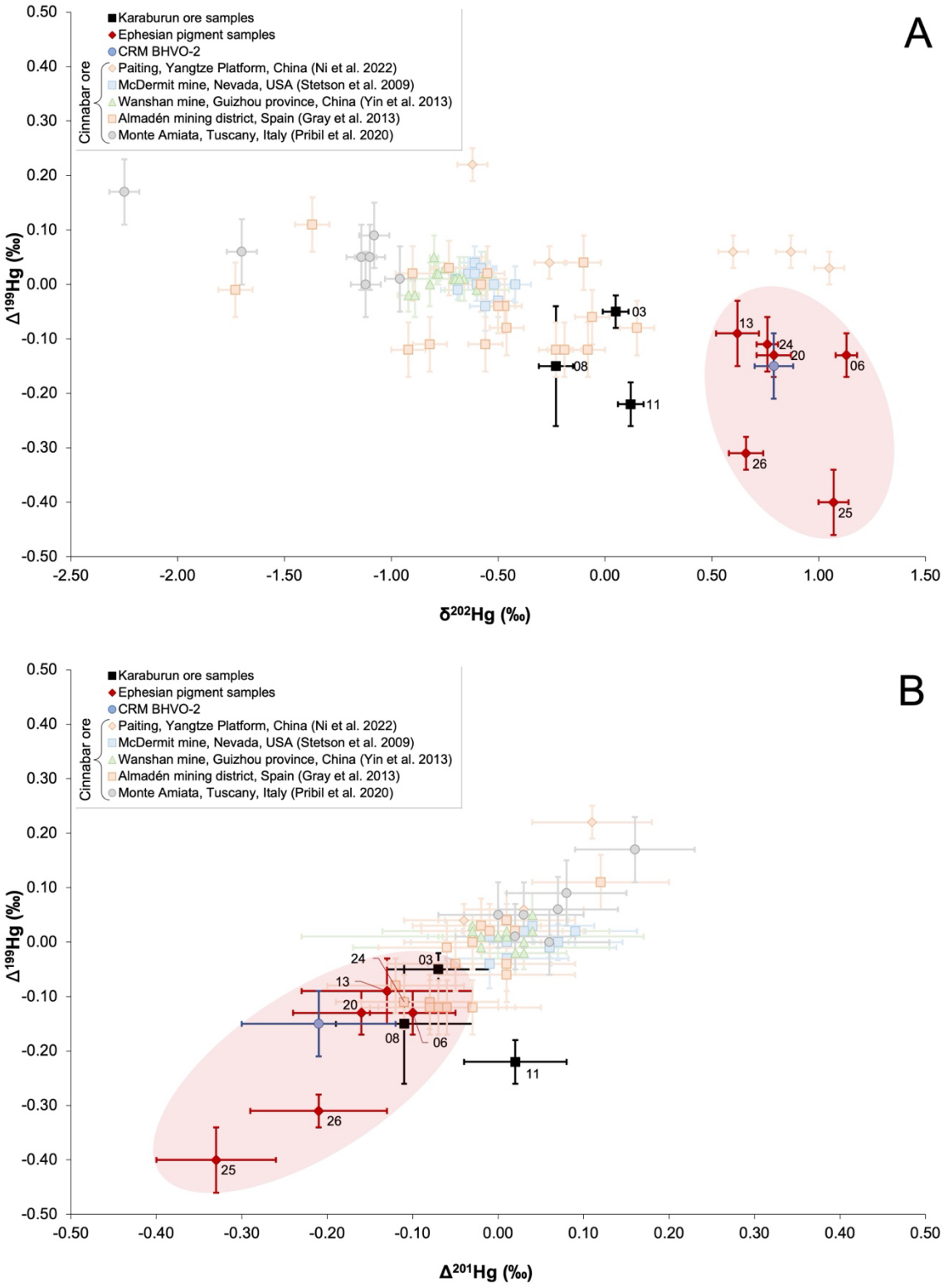


**Figure 7.** Hg isotope ratio data (**A** $\Delta^{199}$Hg *vs* $\delta^{202}$Hg, **B** $\Delta^{199}$Hg *vs* $\Delta^{201}$Hg) for wall painting samples from Ephesus, ore samples from the Karaburun Peninsula, and cinnabar ore samples from Italy (Pribil et al., 2020), Spain (Gray et al., 2013), China (Yin et al., 2013; Ni et al., 2022), and USA (Stetson et al., 2009). (2-column fitting image)